TU DELFT

BACHELOR THESIS

APPLIED PHYSICS AND MATHEMATICS

Connecting the dots: High field ballistic supercurrents

Author:
Hidde Dijkstra

Supervisors:
Dr. Anton Akhmerov
Dr. Joris Bierkens

March 14, 2018

Abstract

We provide the theory and numerical tools required to simulate Josephson current at high magnetic fields. We study the flow of supercurrents between two superconducting contacts connected by a 2d layer of graphene. At uniform fields electrons and holes follow circular trajectories within the graphene layer. When an electron crosses the interface between grahene and one of superconductors it retro-reflects into a hole. When a combination of reflections leads to a loop we have an Andreev bound state. We use the Markov chain Monte Carlo method provided by the Python package emcee to find these Andreev bound states. Using sample trajectories we estimate the current as a function of the superconducting phase difference between the contacts and the magnetic field.

Voorwoord

Deze thesis is de afsluiting van mijn dubbele bachelor studie aan de TU Delft. Aangezien het een dubbele bachelor is, is het onderzoek tweeslachtig. Enerzijds bestudeer ik de ontwikkeling van superstromen in uniforme magnetische velden voor de bachelor Technische Natuurkunde. Anderzijds bestudeer ik de mogelijkheid om Markov ketens te gebruiken om fysische resonanties te vinden voor de bachelor Technische Wiskunde. Graag zou ik Anton willen bedanken dat hij me met een kluitje het riet heeft ingestuurd en Joris dat hij me er daarna weer uit heeft gehaald.

Contents

Introduction

In 1962 Brian David Josephson found a physical explanation for a slightly unusual phenomenon: a finite current between two superconductors separated by a thin insulator. Josephson argued that current flows in the presence of a complex phase difference $\Delta\phi$ between the superconductors. By applying continuity of the wavefunction at both interfaces he reasoned that the current has sinusoidal dependency on $\Delta\phi$:

$$I(\Delta\phi) = I_c \sin(\Delta\phi), \tag{1.1}$$

I_c is a system dependent quantity known as the critical current.[1] It depends on the usual stuff: insulator thickness, electron density, and physical constants. We set the $\hbar$ low and show a picture of the Josephson current in figure 1.2 for future reference.

The situation becomes more interesting when we replace the insulator by a conducting material: a metal or a doped semiconductor. We recall that doping is the process of adding impurities to a material. These impurities either steal electrons from the surrounding material or surrender their own. With this extra boost materials such as graphene become conductive.

Conductive barriers between superconductors are less resistive to electrons tunneling through them. For a superconductor-normal metal-superconductor junction (SNS) the distance between the superconductores can be larger without totally impeding the current. We replace the 1d insulator in figure 1.1 by a conducting material with a 2d geometry (see figure 1.3).

With this new degree of freedom come new interesting physical possibilities. Superconductors expel magnetic fields by virtue of the Meissner effect[2] but conductors do not. By increasing the distance between superconductors we allow the presence of a uniform magnetic field $\mathbf{B}$. If the system is large compared to the penetration depth of magnetic fields we can approximate an in plane magnetic field as a step function:

$$\mathbf{B}(\mathbf{x}) = \begin{cases} B\hat{z} & \text{for } \mathbf{x} \text{ in the conductor,} \\ 0 & \text{for } \mathbf{x} \text{ in the superconductor,} \end{cases}$$

which is tidy and gauge invariant.

Sadly quantum mechanics does not care about the magnetic field. It cares about the magnetic vector potential $\mathbf{A}$ defined such that $\nabla \times \mathbf{A} = \mathbf{B}$. This is a bad definition: $\mathbf{A}$ is not uniquely defined. We can rotate and translate $\mathbf{A}$ freely in our 2d geometry and still describe the same field $\mathbf{B}$. The choice of $\mathbf{A}$ is known as the gauge. For us to

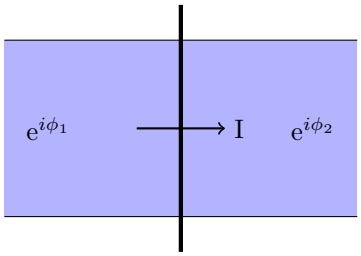

Figure 1.1: Two superconductors separated by a thin insulator. When the two superconductors have a phase difference $\Delta\phi = \phi_1 - \phi_2$ a finite current flows through the insulator: the Josephson current.

[1] Tinkham [4] p. 196.
[2] Tinkham [4] p. 3.

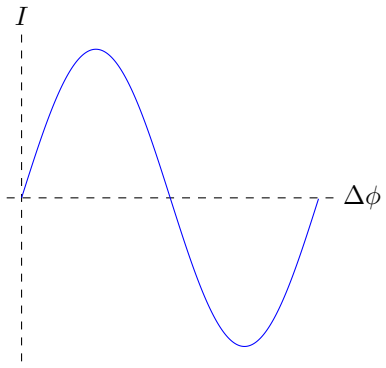

Figure 1.2: The Josephson current through a Josephson junction has a sinuosidal dependency on the phase difference $\Delta\phi$ between the superconductors.

describe the physical world any calculation with $\mathbf{A}$ must be gauge invariant. That is: any choice of $\mathbf{A}$ must yield the same result.

To this end we introduce the gauge invariant superconducting phase difference:[3]

$$\gamma = \Delta\phi + \frac{q}{\hbar}\int \mathbf{A}\cdot \mathrm{d}\mathbf{s},$$

with q the particle charge and $\hbar$ the reduced Planck constant (say h bar). The integral is important and we use it frequently in this report: the Aharonov-Bohm phase.[4]

We are going to cheat and claim that the charge is twice the electron charge $-e$. We can now introduce the flux quantum: $\Phi_0 = h/2e$, with $h = 2\pi\hbar$ the regular Planck constant. The phase difference becomes:

$$\gamma = \Delta\phi - \frac{2\pi}{\Phi_0}\int \mathbf{A}\cdot \mathrm{d}\mathbf{s},$$

with the Josephson current density:

$$j = j_c \sin(\gamma).$$

We switched to the current density because we have made the the phase difference location dependent. Depending on our gauge choice γ varies over the interface.

Since γ is gauge invariant we can choose any gauge. Say we choose $\mathbf{A} = -By\hat{x}$ oriented perpendicular to the interface between the left superconductor and the normal metal. We place the origin of our coordinate system in the middle of the junction and define the width of the interface as W and the length as L. We take the integral over the interface to calculate the total current:

$$\begin{aligned}
I &= \int_{-W/2}^{W/2} j\,\mathrm{d}y = j_c \int_{-W/2}^{W/2} \mathrm{d}y\, \sin\left(\Delta\phi - \frac{2\pi}{\Phi_0}\int_{-L/2}^{L/2} -By\,\mathrm{d}x'\right)\\
&= j_c \int_{-W/2}^{W/2} \mathrm{d}y\, \sin\left(\Delta\phi + \frac{2\pi BL}{\Phi_0}y\right)\\
&= -\frac{j_c}{2\pi BL/\Phi_0}\left[\cos\left(\Delta\phi + \frac{2\pi BL}{\Phi_0}y\right)\right]_{-W/2}^{W/2}\\
&= -\frac{j_c}{2\pi BL/\Phi_0}\left[\cos\left(\Delta\phi + \frac{\pi BLW}{\Phi_0}\right) - \cos\left(\Delta\phi - \frac{\pi BLW}{\Phi_0}\right)\right]\\
&= \frac{j_c}{2\pi BL/\Phi_0} 2\sin\Delta\phi\, \sin\left(\frac{\pi BLW}{\Phi_0}\right)\\
&= j_c W \sin\Delta\phi \,\mathrm{sinc}\left(\pi\frac{\Phi}{\Phi_0}\right),
\end{aligned}$$

where we have used the flux through the normal region: $\Phi = \int B\,\mathrm{d}\mathbf{a} = BWL$ and $\mathrm{sinc}(x) = \sin(x)/x$. For $\Phi = 0$ the current reduces to the Josephson current of equation 1.1.

Apparently the current 'counts' the amount of flux quanta Φ_0 in the system. The pattern that we create by varying the field is the Fraunhofer pattern[5] (see figure 1.4).

[3] Tinkham [4] p. 202.

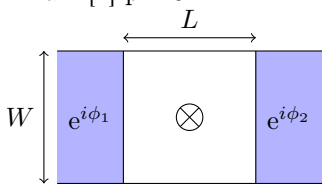

Figure 1.3: Two superconductors seperated by a normal region consisting of a conductor. The normal region has a width W and a length L and an in plane field. Depending on the strength of the field the current going through the junction follows the Fraunhofer pattern.

[4] Kregar [2].

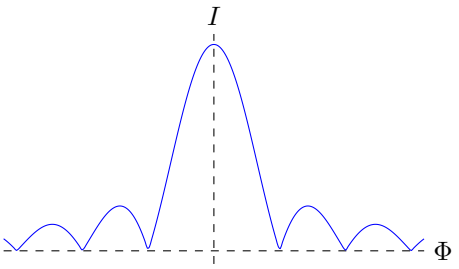

Figure 1.4: The Fraunhofer pattern is the sinc relationship between the current and the flux through a Josephson junction. At regular intervals of Φ_0 the current dies out creating the oscillatory pattern.

[5] de Leeuw [3].

We can use interference patterns like the Fraunhofer pattern to measure small fields to great precision. At larger fields however the current does not necessarily obey the Josephson current relation. The source of this break down is the Lorentz force. For a uniform magnetic field electron start moving along circular trajectories. In normal metals the cyclotron radius ρ is:

$$\rho = \frac{mv}{eB},$$

with m the electron mass and v the electron velocity.

In graphene however, electrons are 'massless'. Their effective mass is significantly smaller than the usual rest mass m and as such they undergo greater curvature at the same field.[6] To find the cyclotron radius we replace the product of the mass and the velocity by the the Fermi momentum of an electron in graphene: $p_F = \hbar k_F = h/\lambda_F$. These are system specific constants known as the Fermi wavevector and the Fermi wavelength with $k_F = \lambda_F/2\pi$. We rewrite the cyclotron radius in graphene in terms of flux with A the area penetrated:

$$\rho = \frac{p_F}{eB} = \frac{h/\lambda_F}{e\Phi/A} = \frac{2A}{\lambda_F}\left(\frac{\Phi}{\Phi_0}\right)^{-1}. \tag{1.2}$$

Expressing the cyclotron radius as a function of the amount of flux quanta Φ_0 allows for a tidy conversion between the two. In the rest of the report we frequently use the flux instead of the magnetic field. The area A of the junction does not change so the relation is linear.

When the cyclotron radius is much larger than the system size we can neglect the curvature and assume linearity. This is the assumption that underlies the calculations of the Fraunhofer pattern. In this report we go beyond this assumption and build up to the Josephson current from scratch without neglecting curvature. Our goal is to find a junction geometry that has an interference pattern similar to the Fraunhofer pattern at high fields. We start by looking at electron trajectories between two superconducting contacts.

[6] Castro Neto et al. [1].

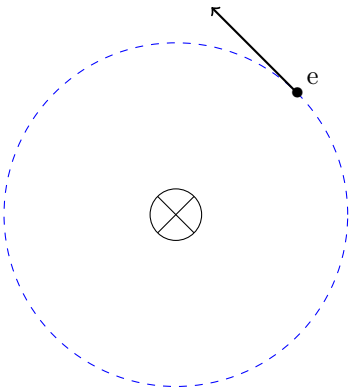

Figure 1.5: An electron follows a circular trajectory in the presence of a uniform magnetic field. When the radius of this trajectory, the cyclotron radius, is much larger than the system size we assume the trajectories to be approximately linear.

References

[1] A. H. Castro Neto et al. "The electronic properties of graphene". In: *Rev. Mod. Phys.* 81.1 (2009).

[2] Ambrož Kregar. *Aharonov-Bohm effect*. 2011.

[3] Joanne de Leeuw. *Fraunhofer Pattern in a 3D Josephson Junction*. 2017.

[4] Michael Tinkham. *Introduction to Superconductivity*. 2nd. Mineola, New York: Dover Publications, Inc., 1996.

Electron trajectories

We discuss how classical electron trajectories between two superconductors form from the Bogoliubov-de Gennes equations. At the interface of a superconductor and a normal metal electrons reflect as holes and holes as electrons. This process is known as Andreev reflection. When a trajectory allows for indefinite exchange of holes and electrons this is called an Andreev state. We integrate over all possible Andreev states to get the Josephson current for a junction. The challenge we tackle is generalizing the existing theory to high magnetic fields: fields which result in cyclotron radii of comparable magnitude to the system size.

2.1 Introduction

We want to learn if and how currents form in Josephson junctions at high uniform magnetic fields. Ideally we want to find a geometry that has a clear interference pattern in its critical current at high fields. Such a device can measure large fields with an uncertainty of just a few flux quanta. The existing theory focuses on linear ballistic trajectories or simple cases of cycloidal trajectories. We expand on this where needed to understand which changes we need to make to describe a high field junction.

2.2 Superconductivity

Superconductivity is the phenomenon that allows materials to carry a current without resistance at low temperatures. These supercurrents carry charge not in the form of single electrons but rather by pairs of electrons called Cooper pairs. These pairs form if the combined energy of the pair is smaller than the energy of two single electrons at the Fermi surface.[1] Intuitively this is strange, how can a pair of two negative particles be energetically favorable? Bardeen, Cooper, and Schrieffer claim in their BCS theory that a Cooper pair starts out as a single electron above the Fermi energy. This electron attracts positive charge in the material in the form of atomic nuclei. Due to their greater inertia they create a trail of positive charge behind the electron. This trail is able to attract another electron which forms an energetically favorable pair with the first.[2]

The minimal difference between the energy of a Cooper pair and two electrons at the Fermi surface is called the superconducting energy gap. This energy is minimal

[1] The Fermi surface is the the barrier between filled and unfilled electron states in a material at zero Kelvin. Electrons at the surface have the highest energy of all electrons: the Fermi energy E_F.

[2] This is the basic assumption of the BCS theory which is the first to successfully describe superconductivity. Tinkham [4] pp. 46-47.

when both electrons have opposed momenta and antisymmetric spin, hence a Cooper pair has the form $(\mathbf{k}\uparrow, -\mathbf{k}\downarrow)$.[3] In other words the energetically favorable state is when the Cooper pair has no effective momentum![4] Summing over the energy gain of all the possible states of this form in respect to the probability of the occupancy gives us the energy gap. We follow the BCS theory in assuming that the attractive potential V is independent of the wavevector of a Cooper pair. The superconducting gap is:[5]

$$\Delta = V \sum_{\mathbf{k}} \langle c_{-\mathbf{k}\downarrow} c_{\mathbf{k}\uparrow} \rangle, \tag{2.1}$$

with $c_{\mathbf{k}\sigma}$ the annihilation operator for an electron with wavevector $\mathbf{k}$ and spin σ. Together these two annihilation operators destroy a Cooper pair. We sum over the expected energy gained by destroying every possible state. The occupancy of these is subject to Fermi-Dirac statistics. As the temperature increases the states with unfavourable energies become more likely: lowering the expected energy gain. At some critical temperature T_c the superconducting gap becomes zero and the material will return to its regular state.

[3] The momentum is related to the $\mathbf{k}$ vector via: $\mathbf{p} = \hbar\mathbf{k}$.

[4] This does not mean that there can be no current. The generalized momentum is $\mathbf{p} = m\mathbf{v} + q\mathbf{A}$: a finite velocity is expected in the presence of a magnetic vector potential.

[5] Tinkham [4] p. 59.

2.3 Bogoliubov-de Gennes

As a starting point for our understanding of superconductivity we use the Bogoliubov-de Gennes equations:[6]

$$\begin{pmatrix} \mathcal{H}_e & \Delta \\ \Delta^* & -\mathcal{H}_e^* \end{pmatrix} \begin{pmatrix} u \\ v \end{pmatrix} = \epsilon \begin{pmatrix} u \\ v. \end{pmatrix} \tag{2.2}$$

The diagonal consists of the Hamiltonian for a single electron $\mathcal{H}_e$ and a single hole $\mathcal{H}_c$. Exciting a hole is equivalent to exciting an electron with opposite momentum and charge so $\mathcal{H}_h = -\mathcal{H}_e^*$.[7] The wavefunctions u and v describe the excitations of electrons and holes respectively. When Δ is zero this set of equations reduces to two separate Schrödinger equations. This is equivalent to there being no superconductivity.

The Hamiltonian of a single electron is:

$$\mathcal{H}_e = -\frac{\hbar^2}{2m}\left(\nabla - \frac{ie}{\hbar}\mathbf{A}\right)^2 + U_{pot}(\mathbf{r}) - \mu. \tag{2.3}$$

We seek to simplify this Hamiltonian by making an approximation known as the semi-classical or WKB approximation. This approximation aims at simplifying a differential equation by writing the solution as an oscillating part multiplied by a function describing an amplitude. If the change in amplitude is gradual compared to the frequency of oscillations then the oscillations will dominate the derivative. Double derivatives in the amplitude are then of negligible importance in the whole differential equation. To this end we introduce the phase factors:

$$\phi_e = \mathbf{k}\cdot\mathbf{r} - \gamma(\mathbf{r}),\ \phi_h = \mathbf{k}\cdot\mathbf{r} + \gamma(\mathbf{r}), \tag{2.4}$$

with $|\mathbf{k}| = k_F$, the Fermi wavevector, and γ the Aharonov-Bohm phase:[8]

$$\gamma = \frac{e}{\hbar}\int_{s_1}^{s_2} \mathbf{A}\cdot \mathrm{d}\mathbf{s}, \tag{2.5}$$

[6] Kopnin [1] p. 35.

[7] A hole is an abstract way of looking at electron excitations. Exciting an electron removes the electron from an energetically favourable state; creating an empty state or hole. Since the existence of a hole is unstable we can view it as an excited particle. It is more convenient to consider a hole moving through a material rather than a sequence of electron pushing each other forward.

[8] Kregar [2].

which we calculate along the particle trajectory. When this trajectory is a closed loop the Aharonov-Bohm phase represents the number of flux quanta[9] enclosed by the loop. The derivative along the trajectory of the Aharonov-Bohm phase cancels out the dependency on the vector potential $\mathbf{A}$ in the Bogoliubov-de Gennes equations since $\partial_t e^{i\gamma} = \frac{ie}{\hbar}\mathbf{A}e^{i\gamma}$.

We use the phase factors to separate the electron and hole wave equations in two parts:

$$\begin{pmatrix} u \\ v \end{pmatrix} = e^{i\phi_e(\mathbf{r})}\begin{pmatrix} U(\mathbf{r}) \\ 0 \end{pmatrix} + e^{i\phi_h(\mathbf{r})}\begin{pmatrix} 0 \\ V(\mathbf{r}) \end{pmatrix}. \tag{2.6}$$

After applying the semi-classical approximation we arrive at the Andreev equations:[10]

$$-i\hbar\mathbf{v}_F \cdot \nabla U + \Delta V = \epsilon U, \tag{2.7}$$
$$i\hbar\mathbf{v}_F \cdot \nabla V + \Delta^* U = \epsilon V. \tag{2.8}$$

2.4 Quantum to classical

In the classical situation we know that electrons in a uniform magnetic field undergo a circular motion with constant velocity due to the Lorentz force. We expect this motion to satisfy the Andreev equations as well. In a conducting material, the so called N region,[11] the superconducting gap is zero so the equations decouple. The only degree of freedom is the angle θ allowing us to replace ∇ by $\frac{1}{\rho}\partial_\theta$ with ρ the cyclotron radius. Putting the approximated Hamiltonian back into the time dependent Schrödinger equation yields a propagating wave differential equation:

$$-\frac{v_F}{\rho}\partial_\theta \Psi' = \partial_t \Psi',$$

where the approximated solution to the time dependent Schrödinger equation is:

$$\Psi = e^{i\phi(\theta)}\Psi'$$

which describes a wave propagating along a circular trajectory; picking up a complex phase on the way. It is this wave that corresponds with the classical notion of a particle (see figure 2.1).

For graphene the dispersion relation[12] is linear close to the Fermi energy. Wave packets in graphene will behave similarly to light which also has a linear dispersion relation. It is this property that inspires the loose classification of electrons in graphene as 'relativistic' or 'massless'.[13] We consider photon like solutions to the differential equation: form-retaining Gaussians which satisfy the Heisenberg uncertainty. For an electron this requires that the uncertainty in momentum $\sigma_\mathbf{p}$ multiplied by the uncertainty in position $\sigma_\mathbf{r}$ is larger than the Planck constant divided by two:

$$\sigma_\mathbf{r}\sigma_\mathbf{p} \geq \frac{\hbar}{2} \Leftrightarrow \sigma_\mathbf{r}\sigma_\mathbf{k} \geq \frac{1}{2}. \tag{2.9}$$

We expect these uncertainties to be related to the Fermi wavelength[14] and the Fermi wavevector respectively. Assuming $\sigma_{rel} \sim \lambda_F$ and $\sigma_\mathbf{k} \sim k_F/4\pi$ we have wave packets with minimal uncertainty.

[9] One flux quantum Φ_0 is defined as $h/2e$ with $h = 2\pi\hbar$, it is the flux of one Cooper pair (charge $2e$) in a circular motion.

[10] We use $U_{pot}(\mathbf{r}) \approx 0$ since we do not intend on using a gate in the future and $\mu \approx E_F = k_F^2\hbar^2/2m$ since we are at sufficiently low temperatures. We give a more thorough derivation in the appendix under WKB approximation.

[11] N for normal metal. In our case we use graphene for its simple dispersion relation (even though it is not a metal).

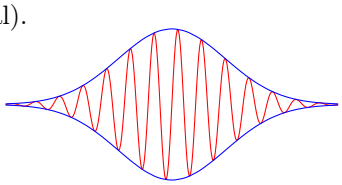

Figure 2.1: A visualization of the real part of the solution Ψ. We understand the particle nature of an electron by its Gaussian envelope. In the semi-classical approximation we neglect the fluctuations in the envelope in favor of the fluctuations in the complex phase.

[12] The dispersion relation is the relation between the wave frequency ω and the wavevector k. When this relation is not linear the initial wave will disperse and change shape.

[13] Qinlong [3].

[14] The Fermi wavelength λ_F is equal to $2\pi/k_F$.

We are now able to describe an electron and its wavefunction for a circular segment but what happens when it encounters an inhomogeneity? There are two instances where this happens in our set-ups: the interface between the N region and an insulator and the interface with a superconductor.

Specular reflection

At the interface between the N region and an insulator the superconducting gap Δ is zero in both materials. As a result we can treat the Andreev equations (2.7) and (2.8) as two separate differential equations just like before. The difference with the previous assessment is that an electron is not able to exist in the insulating region. The continuity condition on the wavefunction requires the wavefunction to be zero at the boundary. This corresponds with the wave getting reflected with opposite polarity: we add the constant π to the phase ϕ. After reflection the wave packet will continue along a new circular trajectory.

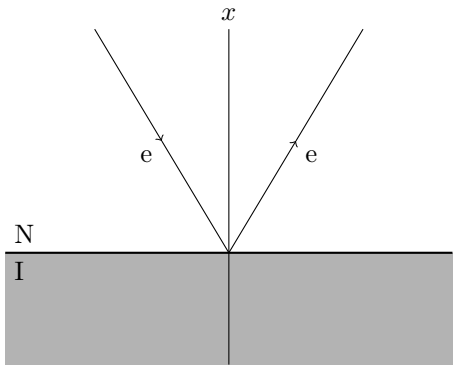

Figure 2.2: I-N interface with incoming electron (e) getting reflected off an insulator. During reflection the complex phase changes sign.

Andreev reflection

The second possible interface in our systems are between graphene and superconductors. We assume that the Fermi velocity is equal in both materials and there is no insulating layer in between. In short we do not consider the possibility of possible refraction/reflection from these sources. We address the interface in a length scale where the cycloidal trajectories are approximately linear and the superconducting gap is a step function:

$$\Delta(x) = \begin{cases} \Delta_0 \mathrm{e}^{i\phi_\mathrm{S}/2} & x < 0, \\ 0 & x > 0, \end{cases} \tag{2.10}$$

with Δ_0 a constant gap energy and ϕ_S the superconducting phase. We choose the x-axis to be paraxial with the S-N interface as shown in figure 2.3. Since the Fermi velocity is equal in both materials there will be no refraction. If the particle is able to enter the superconductor it will continue at the angle of incidence.[15] We parametrize the solution along this angle:

$$-i\hbar v_F \partial_t U + \Delta V = \epsilon U, \tag{2.11}$$
$$i\hbar v_F \partial_t V + \Delta^* U = \epsilon V. \tag{2.12}$$

Since we assumed linearity v_F retains its orientation in these equations. In the region $x > 0$ the equations are once more decoupled so we get unnormalized solutions:

$$\begin{pmatrix} U \\ V \end{pmatrix}_N \propto \mathrm{e}^{i\lambda_N t} \begin{pmatrix} 1 \\ 0 \end{pmatrix} + \mathrm{e}^{-i\lambda_N t} \begin{pmatrix} 0 \\ a \end{pmatrix} \tag{2.13}$$

with $\lambda_N = \epsilon/\hbar v_F$. The constant a is a complex number which regulates the probability of a hole getting reflected.

In the superconducting region the wave functions become decaying exponentials for $\epsilon < \Delta_0$.

$$\begin{pmatrix} U \\ V \end{pmatrix}_S \propto \mathrm{e}^{-\lambda_\mathrm{S} t} \begin{pmatrix} U_0 e^{i\phi_\mathrm{S}/2} \\ V_0 e^{-i\phi_S/2} \end{pmatrix} \tag{2.14}$$

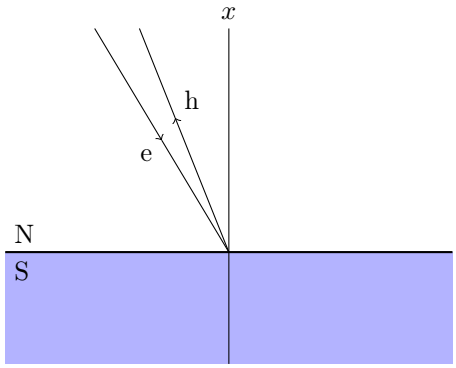

Figure 2.3: S-N interface with incoming electron (e) getting retro-reflected into a hole (h). The momentum of the hole is not exactly equal to that of the electron. This difference is negligibly small compared to the Fermi energy: we treat the incidence angle and angle of refraction as equal.

[15] There is no field in a superconductor due to the Meissner effect so the electron trajectory is not subject to the Lorentz force.

with $\lambda_S = \sqrt{\Delta_0^2 - \epsilon^2}/\hbar v_F$ and U_0 and V_0 the superconducting coherence factors:[16]

$$U_0 = \frac{1}{\sqrt{2}}\left(1 + i\frac{\sqrt{\Delta_0^2 - \epsilon^2}}{\epsilon}\right)^{1/2},$$
$$V_0 = \frac{1}{\sqrt{2}}\left(1 - i\frac{\sqrt{\Delta_0^2 - \epsilon^2}}{\epsilon}\right)^{1/2}.$$

Apparently an incoming electron is not able to enter the superconductor when it has energy smaller than the superconducting gap. In retrospect this is not surprising: the gap is defined as the energy an electron gains when forming a Cooper pair. This electron had to start in some state that is now available to electrons coming in from the N-region. It has to form a Cooper pair to proceed and this happens by pulling another electron from the N-region. This electron leaves behind a hole: the reflected hole in the non-coupled equation (2.13). The hole moves in the opposite direction as the incident electron and so conserves momentum. This form of reflection is known as Andreev reflection or retro-reflection (see figure 2.3).

[16] Kopnin [1] p. 53.

2.5 Andreev bound states

The question on everyone's mind now of course is what happens when we combine two superconducting contacts to a 2d graphene geometry. A simple example is the long Josephson junction seen in figure 2.4. At small fields the electrons and holes travel between superconductors in linear trajectories and form Andreev bound states. A bound state is a trajectory which allows electron and holes to be exchanged indefinitely. At zero field in the long junction every starting position and angle results in a bound state since the hole perfectly retraces the path of the electron and vice versa.

Each bound state has an energy associated with it. This energy results from continuity of the wavefunctions at the interfaces. For linear trajectories in a small magnetic field this energy does not depend directly on the Fermi wavevector because the hole and electron trajectories have identical length. It depends on the Aharonov-Bohm phase[17] γ as well as on the phase difference between both superconductors: $\phi_{S_2} - \phi_{S_1}$. We have:[18]

$$\epsilon = \pm\hbar(T_{S\text{-}S})^{-1}\left[\frac{\phi_{S_2} - \phi_{S_1} - \gamma}{2} \mp \arcsin\frac{\epsilon}{\Delta_0} + \pi\left(l \pm \frac{1}{2}\right)\right], \tag{2.15}$$

with $T_{S\text{-}S}$ the time it takes for an electron or hole to travel between contacts. For short junctions this time is small and the energy is proportional to the cosine of $(\phi_2 - \phi_1 - \gamma)/2$.

The energy of a bound states determines its occupancy and as such its ability to carry current from one superconductor to another. Each bound state has a probability of being occupied proportional to the Fermi function f_n for energy ϵ_n. The total

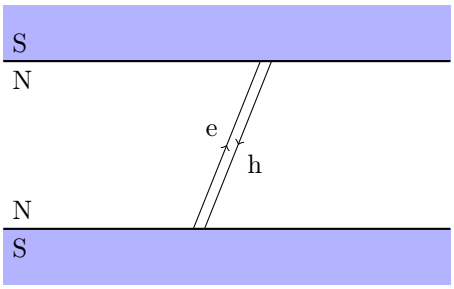

Figure 2.4: The short Josephson junction is a rectangular geometry enclosed by two wide superconducting contacts. At zero field electron and holes are free to bounce between the contacts and form Andreev bound states.

[17] When the hole perfectly retraces the electron γ_e is equal to γ_h.
[18] Kopnin [1] p. 55.

current density is proportional to the sum over all bound states:[19]

$$\mathbf{j} = -\frac{i\hbar e}{m}\sum_n \left[f_n u_n^*(\mathbf{r}) \left(\nabla - \frac{ie}{\hbar}\mathbf{A} \right) u_n(\mathbf{r}) + (1-f_n) v_n(\mathbf{r}) \left(\nabla - \frac{ie}{\hbar}\mathbf{A} \right) v_n^*(\mathbf{r}) - c.c. \right], \tag{2.16}$$

with *c.c.* the complex conjugate.

We reuse the semi-classical approximation and only consider the derivatives in respect to the phase factors ϕ_e and ϕ_h:

$$\mathbf{j} = e\sum_n (\mathbf{v}_F)_n [f_n |U_n|^2 - (1-f_n)|V_n|^2], \tag{2.17}$$

where the Fermi velocity has an orientation depending on the bound state. Once again we return to the semi-classical approximation and consider the complex phase in u and v to dominate the derivative.

Until now we have only discussed old theory. We wish now to expand the theory to a situation with high magnetic field. Electrons and holes make circular motion in a uniform magnetic field due to the Lorentz force. The trajectory an electron follows when travelling from one superconductor to the second differs from the trajectory the reflected hole follows. In figure 2.5 we see that forming an Andreev bound state is no longer trivial. We need to make sure that holes come back to the same position as the electrons started!

But what does it mean to come back to the original position? To answer this we go back to our description of electrons and holes as Gaussian wave packets. The uncertainty in the position and momentum of an electron allows its wavefunction to overlap with that of the electron which is the Andreev reflection of the returning hole. The probability of accepting a trajectory is equal to the overlap of the two wavefunctions. The initial wavefunction ψ_i along the S-N interface is approximately equal to $A\exp(-x^2/4\sigma_x^2)$ and the wavefunction of the returned Andreev reflected electron is $\psi_r = A\exp(-(x-\Delta x)^2/4\sigma_x^2)$. Δx is the distance between begin and end point along the contact. The acceptance chance in position is:

$$\begin{aligned} P_{\text{pos}} &= \int \psi_r^* \psi_i \,\mathrm{d}x = A^2 \int \exp\left(-\frac{1}{4\sigma_x^2}[(x-\Delta x)^2 + x^2] \right) \mathrm{d}x \\ &= A^2 \int \exp\left(-\frac{1}{4\sigma_x^2}[2(x-\Delta x/2)^2 + \Delta x^2/2] \right) \mathrm{d}x \\ &= \mathrm{e}^{-\Delta x^2/8\sigma_x^2} A^2 \int \exp\left(-\frac{(x-\Delta x/2)^2}{2\sigma_x^2} \right) \mathrm{d}x \\ &= \mathrm{e}^{-\Delta x^2/8\sigma_x^2}. \end{aligned}$$

We combine this with a similar derivation for the acceptance chance in respect to momentum to acquire:

$$P(\text{Andreev}) = \exp\left(-\frac{\Delta x^2}{8\sigma_x^2} - \frac{\Delta k^2}{8\sigma_k^2} \right). \tag{2.18}$$

[19] Kopnin [1] p. 58.

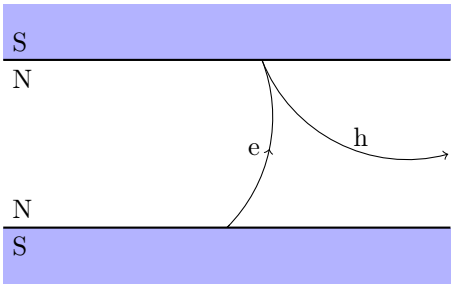

Figure 2.5: In high magnetic fields electrons and holes follow circular trajectories. For most starting angles they do not form Andreev states because the holes do not come back to the starting position of the electrons.

2.6 High field Andreev energies

The equation for the Andreev energy given by (2.15) is not valid for non-linear trajectories. We need to go back to the Andreev equations and look at the solutions more generally. Say we have some trajectory of an electron going from superconductor S_1 to superconductor S_2 with a hole returning to the same position at the same angle as seen in figure 2.6. The length of the electron and hole trajectories are respectively d_e and d_h. The solutions to the Andreev equations in both regions allow for a phase shift along the trajectory. In the N region we can shift both electron and hole phase independently but in the S region they are coupled.

We shift the solutions at superconductor S_1 so that the complex exponent in u and v is real at the interface. It is also important to note that the superconducting phase ϕ_S is not necessarily constant at the interface. This depends on the gauge choice for $\mathbf{A}$ and the geometry of the superconducting contact. We study the consequences in the Implementation chapter.

If A is the normalization constant in the N region and C_1 in the S_1 region then continuity requires:[20]

$$A\begin{pmatrix}1\\a\end{pmatrix} = \begin{pmatrix}u\\v\end{pmatrix}_{N|S_1} = \begin{pmatrix}u\\v\end{pmatrix}_{S_1|N} = C_1\begin{pmatrix}V_0 e^{i\phi_{S_1}/2}\\U_0 e^{-i\phi_{S_1}/2}\end{pmatrix}, \tag{2.19}$$

similary at the second interface with normalization C_2 in the S_2 region:

$$A\begin{pmatrix}e^{i[\phi_e+\lambda_N d_e]}\\ae^{i[\phi_h-\lambda_N d_h]}\end{pmatrix} = \begin{pmatrix}u\\v\end{pmatrix}_{N|S_2} = \begin{pmatrix}u\\v\end{pmatrix}_{S_2|N} = C_2\begin{pmatrix}U_0 e^{i\phi_{S_2}/2}\\V_0 e^{-i\phi_{S_2}/2}\end{pmatrix}. \tag{2.20}$$

By dividing the electron and hole wave equations by each other we drop the normalization constants:

$$\frac{U_0}{V_0}e^{-i\phi_{S_1}} = a = \frac{V_0}{U_0}e^{-i\phi_{S_2}}e^{i(\phi_e-\phi_h)+i\lambda_N(d_e+d_h)}.$$

The quantity U_0^2/V_0^2 is purely a complex phase:

$$\begin{aligned}\frac{U_0^2}{V_0^2} &= \frac{\epsilon+i\sqrt{\Delta_0^2-\epsilon^2}}{\epsilon-i\sqrt{\Delta_0^2-\epsilon^2}}\\ &= \frac{(\epsilon+i\sqrt{\Delta_0^2-\epsilon^2})^2}{(\epsilon-i\sqrt{\Delta_0^2-\epsilon^2})(\epsilon+i\sqrt{\Delta_0^2-\epsilon^2})}\\ &= \frac{(\epsilon+i\sqrt{\Delta_0^2-\epsilon^2})^2}{\epsilon^2+(\Delta_0^2-\epsilon^2)}\\ &= \left(\frac{\epsilon}{\Delta_0}+i\sqrt{1-\left(\frac{\epsilon}{\Delta_0}\right)^2}\right)^2\\ &= \exp\left[2i\arccos\left(\frac{\epsilon}{\Delta_0}\right)\right].\end{aligned}$$

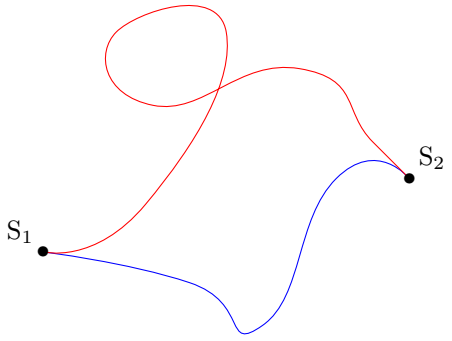

Figure 2.6: A non-linear trajectory for an electron from a superconductor S_1 to a superconductor S_2 in red with corresponding hole trajectory in blue. The trajectories have unequal length so there will be a contribution from k_F in the complex phase.

[20] The superconducting coherence factors switch places compared to equation (2.14) since at the $S_1|N$ interface a hole reflects to an electron instead of an electron to a hole.

We equate the angles which is an implicit definition of the Andreev energy ϵ:

$$2\arccos\left(\frac{\epsilon}{\Delta_0}\right) = \phi_{S_1} - \phi_{S_2} + \phi_e - \phi_h + \frac{\epsilon}{\hbar v_F}(d_e + d_h) + 2\pi l, \tag{2.21}$$

which reduces to the theoretical energies of equation (2.15) for linear trajectories.

2.7 Current

The last step before we can calculate the supercurrent is determining the normalization constants A, C_1, and C_2. The requirement for normalization is:

$$\int (|u|^2 + |v|^2)\mathrm{d}t = 1.$$

In the N-region the wavefunctions consist only of complex phase factors which do not affect the integral: the contribution here is $|A|^2(d_e + d_h)$.[21] The contributions from both S-regions are equal: $|C_1|^2(2\lambda_S)^{-1}(|U_0|^2 + |V_0|^2)$. Continuity of the modulus of the wavefunctions at the interfaces requires: $|A|^2 = |C_1|^2|V_0|^2$. The resulting normalization is:

$$|A|^2 = \frac{1}{d_e + d_h + 2\lambda_S^{-1}} = \frac{\sqrt{\Delta_0^2 - \epsilon^2}}{2\hbar v_F + (d_e + d_h)\sqrt{\Delta_0^2 - \epsilon^2}}. \tag{2.22}$$

[21] The modulus of the complex constant a is 1 since $|U_0/V_0| = 1$.

We use equation 2.17 to express the current density in an arbitrary geometry at high fields in the N-region:

$$\begin{aligned}
\mathbf{j} &= e\sum_n (\mathbf{v}_F)_n[f_n|U_n|^2 - (1-f_n)|V_n|^2] \\
&= -e\sum_n (\mathbf{v}_F)_n|A_n|^2(1-2f_n) \\
&= -e\sum_n (\mathbf{v}_F)_n|A_n|^2 \tanh\left(\frac{\epsilon_n}{2k_BT}\right).
\end{aligned}$$

We integrate along the superconducting contact and exchange the sum for an integral to get the total current:

$$I = \int \mathbf{j}\cdot\mathrm{d}\mathbf{x} \tag{2.23}$$

$$= -e\int \mathrm{d}x_0 \int \mathrm{d}k_x\, P(\text{Andreev})(k_x, x_0)\hat{\mathbf{n}}\cdot\mathbf{v}_F(k_x)|A(\epsilon)|^2 \tanh\left(\frac{\epsilon}{2k_BT}\right). \tag{2.24}$$

The energy depends on x_0 which is the location on the superconducting contact and k_x the wavevector alongside the contact. $\hat{\mathbf{n}}\cdot$ is the normal vector of the interface.

We cannot even solve this integral analytically for simple situations with high fields. We require a numerical approach which finds all trajectories which result in valid Andreev states. For non-chaotic geometries an Andreev state has another Andreev state close it which in turn has another Andreev state close to it et cetera. Contributions to the current come from lines of Andreev states in k_x, x_0 space. Each state in this line has an associated energy which, depending on its sign, interferes with other Andreev states.

2.8 Conclusion

We have found an expression for the current between two superconducting contacts connected by a 2d geometry consisting of graphene. For high magnetic fields we do not know what the Andreev bound states are and how to calculate the associated energies. We require a numerical tool which can find these states however rare and turbulent they might be.

References

[1] Nikolai B. Kopnin. *Theory of Superconductivity*. 1st. Helsinki: Helsinki University of Technology, 2006.

[2] Ambrož Kregar. *Aharonov-Bohm effect*. 2011.

[3] Luo Qinlong. *The elementary electronic properties of graphene*. 2010.

[4] Michael Tinkham. *Introduction to Superconductivity*. 2nd. Mineola, New York: Dover Publications, Inc., 1996.

MCMC

We wish to calculate currents through various geometries as a function of the magnetic field. The total current is an integral over all possible trajectories of an electron through a geometry. In high fields only very few trajectories are valid. The valid trajectories lie along narrow curves as a function of the starting position and direction. A random walk in the form of a Markov chain is used to explore these regions and produce sample trajectories. This kind of method is known as Markov chain Monte Carlo (MCMC). The form we use is called the stretch method as incorporated by the emcee Python package. The samples emcee produces are then used to calculate an estimate of the current for a certain field. The final step consists of normalizing the different estimators compared to each other. We use extended bridge sampling to this end.

3.1 Introduction

Integrating over all trajectories is a difficult task. Most starting conditions will not yield a valid trajectory; either never coming back or never reaching the second superconductor at all. Depending on the geometry and magnetic field the chance of acceptance is a discontinuous function with many snake-like regions of possible trajectories. The rarity of non-zero areas is compounded by the highly oscillatory nature of parts that do contribute to the current. Numerical integration is not an effective tool in our situation. If the algorithm is able to find the areas with contributions to the current it needs to have a step size smaller than half the oscillation period. The result, if correct, will be purely the critical current of the system. Since we want to investigate and understand what happens in various geometries this is hardly enough. We desire knowledge on the precise structure of the allowed trajectories accompanied with information about the phase.

3.2 Monte Carlo integration

A well known alternative to numerical integration is Monte Carlo integration. This method of integration uses an average of function evaluations at random points as an estimator for the value of an integral. More precisely, say we have a function ϕ which we want to integrate over some bounded space A, we wish to know $\int_A \phi \, \mathrm{d}\mathbf{x}$. Instead

of perceiving this integral as the area, volume or a summation of ϕ we can look at it through the lens of probability. We do so by adjusting the format of our integration so it becomes an analogue for the expectation value:[1]

[1] MacKay [4] p. 357.

$$\Phi = \langle \phi(\mathbf{x}) \rangle \equiv \int \mathrm{d}\mathbf{x}\, \pi(\mathbf{x}) \phi(\mathbf{x}), \tag{3.1}$$

where π is a probability distribution.

A straightforward approach is simply taking π to be the uniform distribution in respect to A. We need to make sure π integrates to 1 in our domain. For a uniform distribution acquiring the normalization constant Z is as simple as evaluating $\int_A \mathrm{d}\mathbf{x}$. Knowing Z allows us to write an expression for this π:

$$\pi(\mathbf{x}) = \begin{cases} 1/Z & \text{for } \mathbf{x} \in A, \\ 0 & \text{for } \mathbf{x} \notin A. \end{cases}$$

Inserting this π in expression (3.1) turns it into the integral we wish to evaluate save for a factor $1/Z$. The advantage of this formulation is the possibility of estimating Φ if we have access to a sufficient amount of independent samples from π: $\mathbf{x}_1, ..., \mathbf{x}_N$. For uniform π these are readily available in any modern programming language. We get an estimate for the value of the integral by multiplying the estimate $\hat{\Phi}$ by the normalization constant Z:

$$\int_A \phi \, \mathrm{d}\mathbf{x} = Z \int_A \frac{1}{Z} \phi \, \mathrm{d}\mathbf{x} = Z\Phi \approx Z\hat{\Phi} = \frac{Z}{N} \sum_{i=1}^{N} \phi(\mathbf{x}_i), \tag{3.2}$$

where $\hat{\Phi}$ converges to Φ as N goes to infinity.[2]

[2] In the future we will use $E_i(\phi)$ to denote the expectation value of ϕ with respect to π_i.

3.3 Importance sampling

Often contributions to the integral from ϕ will be local, centered around points or lines. For most $\mathbf{x}$ the contribution to the integral will in practice be negligible. It is inefficient to invest the same amount of computational effort into these 'boring' regions as into regions where ϕ is large. Preferably we are able to instruct our sampler on which areas are more important and need to be sampled more frequently.

In light of this it does not make sense to choose a uniform distribution for π. If ϕ is strictly positive and real the ideal probability to sample is in fact ϕ itself! There will be no samples in regions where ϕ is zero and plenty in regions where ϕ is large. In practice this is difficult. The most glaring difficulty is normalizing ϕ itself; which is just as difficult as the initial problem. Only when we know $\int_B \phi \, \mathrm{d}\mathbf{x}$ for some B we can use this method to estimate the integral for subsets A of B.

This ignores an even more fundamental issue: how do we even acquire independent samples from ϕ? It turns out that this is practically impossible for multidimensional distributions. Intuitively a way of circumventing this problem is using a sum of distributions which we can sample and try to imitate our function ϕ. The main restriction is that we need to have some idea how our function behaves. This is not obvious when there is no explicit expression for ϕ.

What we do know is that the acceptance chance of trajectories behaves like a collection of snake like Gaussians. The acceptance is strictly positive and real, behaving almost like a probability distribution. Unfortunately it suffers from the same issues as mentioned before: we do not know how to get samples from it, let alone how to normalize it. Luckily there is a solution at hand for the first issue.

3.4 Markov chain Monte Carlo

There exists a class of methods for getting samples from some unnormalized probability distribution h with normalization constant Z ($\pi = h/Z$). These methods all share the property that they rely on a random walk to produce samples. A Markov chain performs this random walk so these methods are collectively known as Markov chain Monte Carlo (MCMC). A Markov chain is a sequence of random variables ξ_n such that the chance of moving to a new position ξ_{n+1} depends only on the previous position. This is the famous Markov property:[3]

$$P(\xi_{n+1} = s|\xi_0, ..., \xi_n) = P(\xi_{n+1} = s|\xi_n).$$

[3]Zdzisław [5] p. 88.

We allow this chain to move through a landscape given by h where the chain will be more likely to go to regions which have high values (see figure 3.1). Since this walk is random and each step depends solely on the previous the chain will at some point 'forget' its initial condition. In fact if we wait long enough the chain will forget all its past moves except for a period leading up to the current position. If we take this period to be T we can divide the whole chain in n equal parts with $N = nT$ the total length of the chain. Every of these n points in the path of the chain will be essentially uncorrelated and will adhere to h. By using a Markov chain we are able to create n (pseudo)-uncorrelated samples of h!

Figure 3.1: A Markov chain walks along the landscape of a probability distribution. It compares the current height of the distribution to the height of a possible new position. If the new position is located higher up the hill it is more likely to accept the new position, otherwise it stays in place.

So far so good, but how long should we have to wait till we can call two positions uncorrelated? What is the perfect T and how does this depend on the chance of transition P? If we choose the transition chance badly T will have to be large to compensate. For some Ps the chain will not even behave according to h. If the chain is only allowed to move in a grid pattern the samples we acquire will not follow a continuous distribution. Two properties need to be satisfied for sampling with a Markov chain:[4]

[4]MacKay [4] pp. 372-373.

1. The desired distribution π is an invariant distribution of the chain.

   A distribution π is an invariant distribution of the transition probability $P_t(\mathbf{y}, \mathbf{x})$ if:

   $$\pi(\mathbf{y}) = \int \mathrm{d}\mathbf{x}\, P_t(\mathbf{y}, \mathbf{x})\pi(\mathbf{x}). \tag{3.3}$$

2. The chain must be ergodic, that is:

   $$p^{(t)}(\mathbf{x}) \to \pi(\mathbf{x}) \text{ as } t \to \infty, \text{ for any } p^{(0)}(\mathbf{x}), \tag{3.4}$$

   with $p^{(t)}(\mathbf{x})$ the probability that the chain is at position $\mathbf{x}$ at time t.

The first property demands that if we pick an infinite number of random samples $\mathbf{x}$ from π then the average probability of moving to $\mathbf{y}$ from $\mathbf{x}$ is the same as randomly picking $\mathbf{y}$ from π. This is far from a trivial property; say our transition probability is given by a uniform distribution $P_t = 1/Z$:

$$\pi(\mathbf{y}) = \int \mathrm{d}\mathbf{x}\, P_t(\mathbf{y}, \mathbf{x})\pi(\mathbf{x}) = \int \mathrm{d}\mathbf{x}\, \frac{1}{Z}\pi(\mathbf{x}) = \frac{1}{Z}.$$

This implies that π is constant, which is in general false. We have to be careful choosing P_t.

A method of satisfying this property is using the sufficient requirement of detailed balance. Detailed balance requires the transition probability to obey the rule:

$$P_t(\mathbf{x}_a, \mathbf{x}_b)\pi(\mathbf{x}_b) = P_t(\mathbf{x}_b, \mathbf{x}_a)\pi(\mathbf{x}_a).$$

Using this equality we can exchange $\pi(\mathbf{x})$ for $\pi(\mathbf{y})$ in the integrand of equation (3.3):

$$\pi(\mathbf{y}) = \int \mathrm{d}\mathbf{x}\, P_t(\mathbf{y}, \mathbf{x})\pi(\mathbf{x}) = \int \mathrm{d}\mathbf{x}\, P_t(\mathbf{x}, \mathbf{y})\pi(\mathbf{y}) = \pi(\mathbf{y}) \int \mathrm{d}\mathbf{x}\, P_t(\mathbf{x}, \mathbf{y}) = \pi(\mathbf{y}),$$

satisfying the first property.

Detailed balance itself is satisfied by usage of the Metropolis-Hastings accept chance for moving the Markov chain.[5] Metropolis-Hastings proposes separating P_t into two distinct probabilities: the probability of picking $\mathbf{y}$ as a possible next step: $Q(\mathbf{y}, \mathbf{x})$ and the probability of accepting this $\mathbf{y}$ given $\mathbf{x}$: $p(\mathbf{y}, \mathbf{x})$. Together these probabilities constitute the same quantity as P_t. The Metropolis-Hastings acceptance chance, formulated as:

$$p(\mathbf{y}, \mathbf{x}) = \min\left\{1, \frac{Q(\mathbf{x}, \mathbf{y})\pi(\mathbf{y})}{Q(\mathbf{y}, \mathbf{x})\pi(\mathbf{x})}\right\}.$$

Either $p(\mathbf{y}, \mathbf{x})$ or $p(\mathbf{x}, \mathbf{y})$ is equal to one, the ratio of the two will result in detailed balance. If the move gets accepted the new position of the Markov chain will be $\mathbf{y}$, otherwise the new position will be $\mathbf{x}$. A clear advantage of this formulation is that only the ratio between $\pi(\mathbf{x})$ and $\pi(\mathbf{y})$ is important. The unnormalized distribution h is frequently used in this case since the normalization constant Z disappears after division.

The second condition for MCMC is ergodicity of the Markov chain. Intuitively this means that a chain is able to move from any location to any other. For continuous Gaussian steps ergodicity is achieved an infinite time scale. At finite time scales the related concept of mixing time becomes a problem for multi-modal distributions. If a Markov chain starts in one mode it is unlikely that it will be able to cross towards all other modes within the sampling time. Effectively the chain will remember its initial position because it stays in the initial mode; in contradiction with the required Markov property.

For every MCMC algorithm using the Metropolis-Hastings acceptance chance the most important degree of freedom is the step choice distribution Q. This distribution decides the period required to get (pseudo)-uncorrelated samples. The simplest choice

[5] MacKay [4] p. 366.

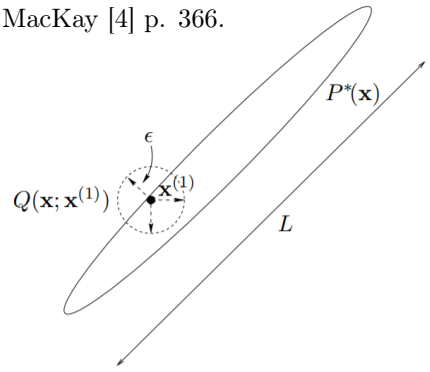

Figure 3.2: A 2d probability distribution P^* with its mode oriented along a line. The step size of the standard Metropolis-Hastings method is confined to a certain constant ϵ. Here this step size is suboptimal, parallel to L a larger step is better and perpendicular a smaller step. The Python package Emcee serves to mitigate this problem. Image from MacKay [4] p. 367.

for Q is only allowing the chain to move in one dimension at a time. For a standard deviation σ we draw a new position from a normal distribution around the current position of the chain. This move is perfectly symmetric since moving back has the same chance as moving to the proposal $\mathbf{y}$: $Q(\mathbf{y}, \mathbf{x}) = Q(\mathbf{x}, \mathbf{y})$. Any location can be reached in a number of steps equal to the dimensionality of π.[6]

We are free to choose any σ beforehand. Choosing a large σ allows the chain to move quickly but has a large rejection rate; the chance of choosing a proposal in a low probability region is high. The inverse: choosing a small σ, leads to a low rejection rate but the chain will only be able to move with small steps. Both require a large period between samples for uncorrelated results, the optimal value will be somewhere in between.

This optimal value will differ per dimension: a narrow Gaussian centered along a line as shown in figure 3.2 will require a small steps size perpendicular to the line and a large one along it. If this line is not oriented in the direction of an axis it will be impossible to take advantage of the proportions of the distribution in choosing σ. This becomes even more difficult if the π is instead centered around a curve.

[6] Disregarding the possibility that π is actually zero at the cross points required for moving to this new position. In this case more steps are required

3.5 Emcee

There is an elegant solution to both our problems: using an ensemble of Markov chains. Each individual chain of the ensemble will only have to visit a couple of modes of a multi-modal distribution for the ensemble to be ergodic. Using uncorrelated chains for the ensemble is possible but not necessary: we can use the current position for other chains in the ensemble to decide the next step for a single chain. Since we only use the current position of the ensemble we retain the Markov property, accordingly the ensemble will still forget its past after a certain period.

During this project I have used a Python module which relies on a correlated ensemble of chains for sampling: the emcee package.[7] This module proposes to move each chain of the ensemble in series (so not parallel) and define the resulting position the state of the ensemble at time $t + 1$.[8] This is required for a correlated ensemble because the move distribution Q becomes a conditional probability depending on the other chains. If the other chains move as well the condition will change accordingly, which results in the move back becoming impossible. The Metropolis-Hastings accept chance will become zero, breaking the ergodicity requirement for the ensemble.

Emcee uses an ensemble of K Markov chains $\mathbf{X} = \{\mathbf{x}_1, .., \mathbf{x}_K\}$. For every k in $\{1, ..., K\}$ sequentially we evolve $\mathbf{X}$ by proposing a move for chain $\mathbf{x}_k$ depending on a randomly chosen chain $\mathbf{x}_j$ with $j \neq k$. After a certain amount of iterations we expect all chains to be in a mode of the distribution π. Assuming these modes are one dimensional, that is they consist of curves in $\mathbb{R}^N$, then we expect all chains to align with these curves. When there are many more chains than modes we can perceive modal curves as a combination of linear segments, each segment containing multiple chains. If we move $\mathbf{x}_k$ along the linear superposition of itself and another chain in the same segment then the chance is high that we will hit another point close to the mode. A greater acceptance rate causes a decline in auto-correlation time improving the performance of the MCMC algorithm. Unfortunately there is no easy way of

[7] Foreman et al. [1].

[8] Practically this means that a single move of the ensemble is actually a collection of K moves of the individual chains

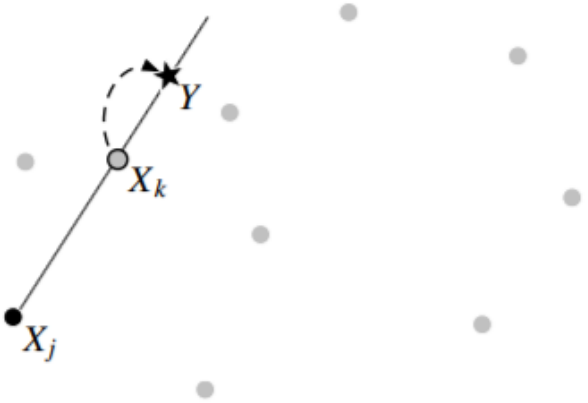

Figure 3.4: The stretch move from $\mathbf{x}_k$ to a proposal $\mathbf{y}$ by taking a linear superposition between $\mathbf{x}_k$ and random $\mathbf{x}_j$. $\mathbf{y}$ is chosen around $\mathbf{x}_k$ using a bounded inverse root as a probability distribution. Image from Goodman [2] p. 70.

picking a chain in the same segment without causing a bias. Emcee picks chains at random and assumes that if we keep doing this we will get enough chains in the same segment for computational gain.

The linear superposition of $\mathbf{x}_k$ with some other chain $\mathbf{x}_j$ is used for the so called stretch move shown in figure 3.4. This move results in a proposal $\mathbf{y}$ using the formula:

$$\mathbf{y} = \mathbf{x}_j + Z(\mathbf{x}_k - \mathbf{x}_j). \tag{3.5}$$

The random component of the stretch move is contained in Z. Z is a stochastic variable drawn from the distribution g:

$$g(z) \propto \begin{cases} \frac{1}{\sqrt{z}} & \text{for } z \in \left[\frac{1}{a}, a\right], \\ 0 & \text{otherwise,} \end{cases}$$

with a some constant greater than one.

All other chains besides $\mathbf{x}_k$ retain their position resulting in a proposal $\mathbf{Y}$ with only one chain changed. The Metropolis-Hastings accept chance p for the ensemble is:

$$p = \min\left\{1, \frac{Q(\mathbf{Y},\mathbf{X})}{Q(\mathbf{X},\mathbf{Y})}\frac{\Pi(\mathbf{Y})}{\Pi(\mathbf{X})}\right\} = \min\left\{1, \frac{q(\mathbf{y},\mathbf{x}_k)}{q(\mathbf{x}_k,\mathbf{y})}\frac{\pi(\mathbf{y})\prod_{j\neq k}\pi(\mathbf{x}_j)}{\pi(\mathbf{x}_k)\prod_{j\neq k}\pi(\mathbf{x}_j)}\right\}.$$

We are able to exchange the move distribution Q for the ensemble by the move distribution q for a single chain. The stretch move (3.5) has a symmetry to it: $\mathbf{y}-\mathbf{x}_j = Z(\mathbf{x}_k-\mathbf{x}_j)$. The important quantities are the distance to $\mathbf{x}_j$ and the chance of picking Z and respectively $1/Z$.[9] The distance maps the distribution g to q: it stretches or contracts the probability distribution q. This deformation needs to be corrected in order to correctly express the ratio $q(\mathbf{y},\mathbf{x}_k)/q(\mathbf{x}_k,\mathbf{y})$ (see figure 3.3). Fortunately we stretch the distribution equally in all dimensions proportional to the distance. If the dimensionality of our distribution is N we have to correct the probability of the move to $\mathbf{y}$ by $||\mathbf{x}_k - \mathbf{x}_j||^N$ and the other way around by $||\mathbf{y} - \mathbf{x}_j||^N = Z^N||\mathbf{x}_k - \mathbf{x}_j||^N$.

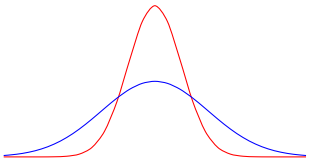

Figure 3.3: When we stretch a probability distribution in one dimension by a we need to reduce the height of the stretched distribution by $1/a$ to retain normalization. A stretch in N dimensions by a requires a factor $1/a^N$ for normalization.

[9] For the move back we have to draw $1/Z$ from g.

Combining this with the equality $zg(z) = g(1/z)$ gives the Metropolis-Hastings accept chance as:

$$\begin{aligned} p &= \min\left\{1, \frac{q(\mathbf{y}, \mathbf{x}_k)}{q(\mathbf{x}_k, \mathbf{y})} \frac{\pi(\mathbf{y})}{\pi(\mathbf{x}_k)}\right\} \\ &= \min\left\{1, \frac{g(Z)/||\mathbf{x}_k - \mathbf{x}_j||^N}{g(1/Z)/||\mathbf{y} - \mathbf{x}_j||^N} \frac{\pi(\mathbf{y})}{\pi(\mathbf{x}_k)}\right\} \\ &= \min\left\{1, Z^{N-1} \frac{\pi(\mathbf{y})}{\pi(\mathbf{x}_k)}\right\}. \end{aligned}$$

As long as the starting position of the ensemble is irreducible in respect to dimensionality the ensemble can move to every position in a finite amount of steps. In respect to the goals of this project this is sufficient to claim ergodicity. The Metropolis-Hastings accept chance guarantees detailed balance so Emcee is a valid MCMC method.

3.6 Extended bridge sampling

Emcee allows us to sample an unnormalized distribution but does not give us information regarding normalization. There is however a method for using the samples generated by emcee for this purpose. Lelièvre [3] puts forth a method of relative normalization in his book on free energy computation. In this book he explains how to compare samples gathered for different energy levels. Energy levels close to each other will show similar behaviour in their distributions. This can be exploited by looking at the intersection of two related distributions: the bridge between them. The percentage of samples of each distribution in the bridge is directly related to the percentage of the volume the bridge takes up of the whole distribution. For two one-dimensional Gaussians this is clearly visible: figure 3.5 shows that the shared region in blue takes up a larger part of the area of the orange Gaussian. Using the samples we can calculate just what these two percentages are and how to calculate the respective normalizations ratio Z_2/Z_1. We go back to the equation for the estimate (3.2) to derive the estimator equation for this value:

$$\frac{Z_2}{Z_1} = \frac{Z_2}{Z_1} \frac{\int \alpha\pi_1\pi_2 \, \mathrm{d}\mathbf{x}}{\int \alpha\pi_1\pi_2 \, \mathrm{d}\mathbf{x}} = \frac{\int \alpha\pi_1 h_2 \, \mathrm{d}\mathbf{x}}{\int \alpha h_1\pi_2 \, \mathrm{d}\mathbf{x}} = \frac{E_1(\alpha h_2)}{E_2(\alpha h_1)} \approx \frac{\frac{1}{n_1}\sum_{i=1}^{n_1} \alpha(\mathbf{x}_i^1) h_2(\mathbf{x}_i^1)}{\frac{1}{n_2}\sum_{j=1}^{n_2} \alpha(\mathbf{x}_j^2) h_1(\mathbf{x}_j^2)}, \tag{3.6}$$

with α an arbitrary function of our choosing which can stress a certain area. We sum over the samples provided by the emcee algorithm for π_1 and π_2: $\mathbf{x}_1^1, ..., \mathbf{x}_{n_1}^1$ and $\mathbf{x}_1^2, ..., \mathbf{x}_{n_2}^2$ respectively.

This expression is not magic and requires that there is a bridge between the two distributions. As the bridge becomes smaller the product $\pi_1\pi_2$ will approach zero. Surprisingly, numerical methods do not like dividing zero by zero. Anybody using this method will have to be well aware this risk. We intend on sampling the conductance for magnetic fields with small steps in between. For a step of one magnetic flux quanta we do not expect radical changes in the way trajectories are distributed.

Lelièvre et al. [3] expands this method to N unnormalized probability distributions h_i: extended bridge sampling. Equation (3.6) becomes a matrix equation

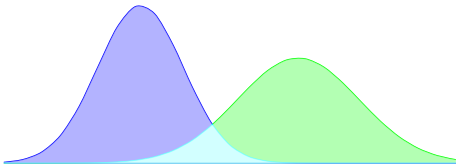

Figure 3.5: Two unnormalized probability distributions in blue and green respectively. Their shared area in cyan can be used to compute their relative normalization. Comparing the percentages of samples from each distribution which are in this area gives an estimate for Z_2/Z_1.

with $Y = (y_2, ...y_N)^T$ the normalization vector. Each y_i is defined as the normalization Z_i/Z_1. We use an iterative method suggested by Lelièvre which we work out thoroughly in the appendix. We start by collecting all samples in one set: $\mathbf{X} = \{\mathbf{x}_1^1, ..., \mathbf{x}_{n_1}^1, ..., \mathbf{x}_1^N, ..., \mathbf{x}_{n_N}^N\}$ with a total number of samples $n = \sum n_j$. Our initial guess for Y is that all normalization constants are equal: $Z_1 = Z_2 = ... = Z_N$; all y_i^1 are equal to one. The next iteration is given by:

$$y_i^{k+1} = \sum_{m=1}^{n} \frac{h_i(\mathbf{X}_m)}{\sum_{j=1}^{N} n_j (y_j^k)^{-1} h_j(\mathbf{X}_m)}. \tag{3.7}$$

After each iteration we normalize all y_i^{k+1} by the result found for y_I^{k+1} with h_I a distribution where we expect a resonance effect. We can use regular Monte Carlo integration to get an approximate normalization constant Z_I for this field. The normalization ratios given by extended bridge sampling can then be used to normalize all other distributions.

3.7 Conclusion

We can now find valid trajectories in any geometry at any field. All that is left is to test various geometries which are likely to support a current. Most likely geometries have certain resonance fields where the current peaks. MCMC combned with extended bridge sampling is perfect for simulating the decay of these currents around the peaks.

References

[1] Daniel Foreman-Mackey et al. "emcee: The MCMC Hammer". In: *PASP* 125.925 (2013).

[2] Jonathan Goodman and Jonathan Weare. "Ensemble samplers with affine invariance". In: *CAMCoS* 5.1 (2010).

[3] Tony Lelièvre, Mathias Rousset, and Gabriel Stolz. *Free Energy Computations*. 1st. London: Imperial College Press, 2010.

[4] David J.C. MacKay. *Information Theory, Inference, and Learning Algorithms*. 18th. Cambridge: Cambridge University Press, 2003.

[5] Brzeźniak Zdzisław and Tomasz Zastwaniak. *Basic Stochastic Processes*. 7th. London: Springer-Verlag London Limited, 1999.

Implementation

We convert the physics from the electron trajectories chapter to formulas we use in our numerics. In particular this includes an explicit definition of the Andreev acceptance chance and the Josephson current. Using the first formula we inspect the autocorrelation of a Markov chain for a square and rectangular junction. Finally we look at a circular junction for which almost all possible trajectories are Andreev bound states. Accordingly we decide to sample this geometry uniformly and have zero autocorrelation.

4.1 Introduction

We now have the tools and theory to calculate currents through junctions. Still we do not have a clear picture of what we actually want to study. We want to construct a junction with interference patterns at high fields, but how do we know what geometries work well? Before looking into geometries we translate the physics to numerics; putting it in a mold that our MCMC sampler emcee can understand.

4.2 Andreev accept chance

The Andreev accept chance cannot be given analytically as a function of the starting angle and position. We require an algorithm which for certain starting coordinates calculates the resulting trajectory. When this trajectory comes back to the original superconductor we map the difference in location and angle to a probability according to wave packet uncertainties. The trajectory does not stop here however; it can continue bouncing until it finds a loop with a higher probability.

Theoretically this calls for trajectories with infinite length; an electron is bound to return some time, right? There are however limitations on the 'life-time' of a ballistic trajectory. At some point an electron or hole scatters when it hits an impurity in the conducting material. The expected length an electron travels before scattering is the mean free path l_m. In graphene the elastic mean free path exceeds a micron and depending on the carrier density can reach values of 28 μm![1] We consider the mean free path in our systems to be 2 μm and allow our trajectories to reach lengths of ten micron. The decay in the probability of a trajectory is exponential. When we have reached a length of 10 μm this probability has dropped to $\exp(-10/l_m) = \exp(-5) \approx$

[1] Banszerus et al. [1].

0.005. We truncate the trajectory at this point to save computational power.

Next we need to choose the uncertainty in position and momentum in our trajectory (σ_x and σ_k). As stated in the electron trajectory chapter the product of these uncertainties must be smaller than $1/2$ according to the Heisenberg uncertainty principle. Due to the conical shape of the dispersion relation in graphene[2] the uncertainty in orientation of the trajectory is linearly related to the uncertainty in wavevector: $\sigma_k = 2k_F\sigma_\theta/\pi$. If the uncertainty in position is related to the Fermi wavelength by some factor a and we require minimal uncertainty then:

$$\frac{1}{2} = \sigma_x\sigma_k = 2a\lambda_F k_F\sigma_\theta/\pi = 4a\sigma_\theta.$$

For $a = 1$ the uncertainty is about 7 degrees. We have to balance this uncertainty against the uncertainty in position we want. Our systems have length scales around 1 to 2 μm to satisfy the semi-classical approximation. We take the Fermi wavelength[3] to be 10 nm so choosing $a = 2$ gives a relative uncertainty of about $1/100$ compared to the system. The uncertainty in orientation is then about 3.5 degrees. Both uncertainties are reasonable when considering deterministic trajectories in non-chaotic systems.[4]

The Andreev acceptance chance for a trajectory is:

$$P(\text{Andreev}) = \sum_{i=1}^{n} P(\text{Accept: } i|\text{Reject: } j<i) = \sum_{i=1}^{n} p[i], \tag{4.1}$$

with:

$$p[i] = \exp\left(-\frac{[\Delta x_i]^2}{8\sigma_x^2} - \frac{[\Delta k_i]^2}{8\sigma_k^2}\right)\left(1 - \sum_{j=1}^{i-1} p[j]\right), \tag{4.2}$$

$$= \exp\left(-\frac{[\Delta x_i]^2}{32\lambda_F^2} - (16\Delta\theta_i)^2\right)\left(1 - \sum_{j=1}^{i-1} p[j]\right), \tag{4.3}$$

where every i corresponds to one possibility of forming an Andreev state.

4.3 Raytracing

All that is left for MCMC to work is having an algorithm which can generate the distances and angles required to calculate the accept chances. To this end we wrote a versatile raytracer which accepts any geometry build out of linear and circular arcs (walls). It accepts both linear and circular trajectories and allows for both uniform and Markov sampling.[5]

Figure 4.2 visualizes the method of raytracing. The algorithm calculates the intersection between a circle representing the cyclotron of an electron and the lines and circles which build up the geometry. For combinations of these arcs it is possible to do this analytically. We have also investigated including an electric field but this requires numerically calculating intersections. To keep the trajectory evaluation time low we have opted to disregard electric fields.

[2] The velocity is related to the dispersion relation as $\mathbf{v} = \hbar^{-1}\partial_{\mathbf{k}}E(\mathbf{k})$. Due to the conical dispersion relation as seen in 4.1 the orientation of $\mathbf{k}$ is perpendicular to the velocity. If the uncertainty in the orientation θ is π then the uncertainty in wavevector is $2k_F$ (the other side of the cone).

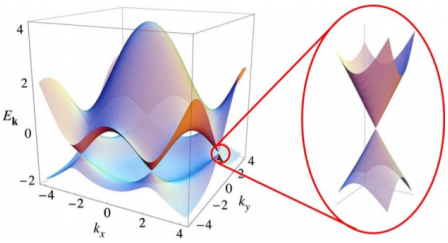

Figure 4.1: Conical dispersion relation of graphene. Image from Castro et al. [3].

[3] The Fermi-wavelength of graphene depends on the density of charge carriers and can be adjusted by doping. We have some liberty in choosing this quantity.

[4] A chaotic system is a system where a small change in initial conditions changes the result drastically. This prevents finite-step approaches from being a good approximation, hence they are also called non-integrable systems.

[5] We have made the code available at [4].

Algorithm 1 Calculating Andreev accept chance of electron trajectory

```
distance travelled ← 0
phase ← 0
walls ← {walls bordering the geometry}
while distance travelled < maximal distance do
    shortest distance ← ∞
    origin ← current position of trajectory
    for wall in walls do
        intersection ← calculate intersection(trajectory, wall)
        distance ← |intersection - origin|
        if distance < shortest distance then
            shortest distance ← distance
            closest wall ← wall
    phase += phase over(shortest distance)
    if closest wall == superconductor then
        Andreev reflect trajectory
        calculate Andreev accept chance
    else
        specular reflect trajectory
    distance travelled += shortest distance
```

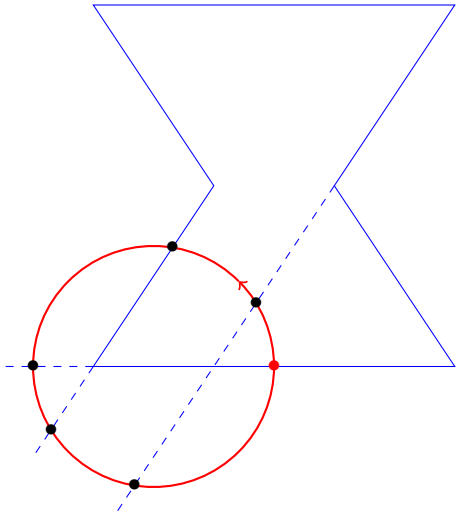

Figure 4.2: The raytracer calculates all intersections with every wall (line segment) in the geometry. For every wall it check whether the intersection is closer to the origin than the previous closest intersection.

The computational labour of the raytracing algorithm lies primarily in solving quadratic equations and applying reflection and rotation matrices. This is in a sense 'dumb work' for which Python is not ideally suited. There exists a module in Python called Cython[6] which combines Python's flexibility with the efficiency of C. It converts specially formatted Python code to C and compiles it. We can then call functions from this code in regular Python code. This is perfect in combination with the emcee package since the computational load required for sampling is negligible. We achieve speed gains of a factor 50 by purely implementing the raytracer in Cython!

[6] Behnel et al. [2].

4.4 Current

We go back to the Andreev energies and current as given in the chapter describing electron trajectories:

$$I = -e \int \mathrm{d}x_0 \int \mathrm{d}k_x \, P(\text{Andreev}) \frac{\hat{n} \cdot \mathbf{v}_F \sqrt{\Delta_0^2 - \epsilon^2}}{2\hbar v_F + (d_e + d_h)\sqrt{\Delta_0^2 - \epsilon^2}} \tanh\left(\frac{\epsilon}{2k_B T}\right),$$

with energies depending on the superconducting phases ϕ_{S} and the phases picked up during the electron and hole trajectories: ϕ_e and ϕ_h:

$$2 \arccos\left(\frac{\epsilon}{\Delta_0}\right) = \phi_{\mathrm{S}_1} - \phi_{\mathrm{S}_2} + \phi_e - \phi_h + \frac{\epsilon}{\hbar v_F}(d_e + d_h) + 2\pi l.$$

We collect all phases in one phase difference: $\Delta\phi = (\frac{1}{2}[\phi_{\mathrm{S}_1} - \phi_{\mathrm{S}_2} + \phi_e - \phi_h])\%\pi$. We take the modulo such that the phase difference lies between 0 and π. The freedom in

l allows us to make this adjustment since we disregard energies larger than the gap. We write the energy now in terms of the gap: $\tilde{\epsilon} = \epsilon/\Delta_0$:

$$\arccos\tilde{\epsilon} = \Delta\phi + \tilde{\epsilon}\frac{\Delta_0(d_e + d_h)}{2\hbar v_F}.$$

The value of $\Delta_0(d_e + d_h)/2\hbar v_F$ dictates which part of the implicit equation for the energy dominates. We estimate this value using a superconducting gap of $3 \cdot 10^{-4}$ eV.[7] In electronvolt-seconds $\hbar$ is roughly $6.6 \cdot 10^{-16}$ eV·s. For a trajectory length of approximately 5 μm we have: $\Delta_0(d_e + d_h)/2\hbar v_F \approx 1$. This means we cannot use the short junction approximation where this value is negligible.[8] Instead we approximate the arccosine with its first order Taylor expansion. Our explicit formula for the energy in respect to the gap becomes:

$$\tilde{\epsilon} = \frac{\pi}{4} - \frac{1}{2}\Delta\phi. \tag{4.4}$$

We disregard the bound state if $|\tilde{\epsilon}| > 1$.

The last step is calculating the phase difference $\Delta\phi$. We separate ϕ_e and ϕ_h in a summation of circle segments with radius R and center (b_x, b_y) from θ_1 to θ_2. We choose the gauge $\mathbf{A} = Bx\,\hat{y}$:

$$\phi_{e,h} = k_F R(\theta_2 - \theta_1) \mp \frac{e}{\hbar}\int_{s_1}^{s_2} \mathbf{A}\cdot \mathrm{d}\hat{l} = k_F R(\theta_2 - \theta_1) \mp \pi\frac{\Phi}{\Phi_0}\int_{\theta_1}^{\theta_2} x(\theta)\frac{\mathrm{d}y}{\mathrm{d}\theta}\,\mathrm{d}\theta, \tag{4.5}$$

using cilyndrical coordinates we have $x = R\cos\theta + b_x$ and $y = R\sin\theta + b_y$:

$$\phi_{e,h} = k_F R(\theta_2 - \theta_1) \mp \pi\frac{\Phi}{\Phi_0}\left[\frac{R^2}{2}\left(\theta + \frac{1}{2}\sin 2\theta\right) + b_x R\sin\theta\right]_{\theta_1}^{\theta_2}. \tag{4.6}$$

When the electron part of trajectory has the same length as the hole part of the trajectory the k_F dependency drops out when taking the difference.

As mentioned in the electron trajectories chapter the superconducting phases ϕ_S are not necessarily constant along the contacts. Weirdly put the superconducting phase must depend on the gauge for the system to be gauge invariant. We can retrace the cause back to the definition of momentum: $\mathbf{p} = m\mathbf{v} + q\mathbf{A}$. There is no current alongside the contact so the velocity in this direction must be zero. Therefore in the semi-classical limit the follow equation must hold:[9]

$$\hbar\partial_t\phi_S \approx \mathbf{p} = q\mathbf{A}.$$

$$\phi_S(t) = \phi_S(0) + \frac{q}{\hbar}\int \mathbf{A}\cdot \mathrm{d}\hat{t}. \tag{4.7}$$

We recognize the last part as the Aharonov-Bohm phase! The charge q is $-e$ for an electron and e for a hole. If we move this phase to ϕ_e and ϕ_h we effectively close the loop relative to some linear reference trajectory between point $t_1 = 0$ on the first superconductor and $t_2 = 0$ on the second superconductor. If the vector potential is oriented perpendicularly to the contact this integral vanishes. For our gauge choice this is true for contacts oriented along the x-axis.

[7] Kittel [6] p. 367

[8] In the short junction limit we can neglect the linear part of the energy equation and simply state $\epsilon = \Delta_0\cos(\Delta\phi)$.

[9] We use $-i\hbar\partial_t = \mathbf{p}$ with the derivative alongside the contact. We replace this operator with the derivative in the complex phase ϕ_S.

Finally we assume $2k_BT >> \epsilon$ so the hyperbolic tangent in the current integrand becomes a sign function for the energy: $\tanh(\epsilon/2k_BT) \approx \sigma(\tilde{\epsilon})$. In our numerics we approximate the current as:

$$I \approx -e \int \mathrm{d}x_0 \int \mathrm{d}k_x \, P(\text{Andreev}) \frac{\hat{n} \cdot \mathbf{v}_F}{d_e + d_h} \frac{\sigma(\tilde{\epsilon})\sqrt{1-\tilde{\epsilon}^2}}{1+\sqrt{1-\tilde{\epsilon}^2}}. \tag{4.8}$$

4.5 Autocorrelation and geometries

Now we know how to calculate the Andreev accept chances and the associated trajectory phases and currents we go back to MCMC. Every N steps we take a sample from the current location from the Markov chain and use these to calculate an expectation value for the current. The choice of N is a balance act: either we choose N too large and we throw away computational time and accuracy or we choose N too small and we risk biasing our estimator. How do we know which N is the right choice?

A measure for the correlation between instances of a random variable is surprisingly called autocorrelation. If the autocorrelation is zero then the instances are independent. For a chain of instances of a random variable such as a Markov chain we want to know how the autocorrelation evolves as a function of N. Instead of looking at the autocorrelation directly we use the autocovariance function and normalize with $C(0)$:

$$C(T) = \lim_{t\to\infty} \mathrm{cov}(X[t+T], X[t]). \tag{4.9}$$

Here $X[t]$ is the instance of a random variable at time t. The limit t to infinity is taken to remove any dependency on the starting condition of X. For a Markov chain with M samples we approximate this function with:[10]

[10] Foreman-Mackey et al. [5].

$$C(T) \approx \frac{1}{M-T} \sum_{m=1}^{M-T} (X[m+T] - \langle X \rangle)(X[m] - \langle X \rangle). \tag{4.10}$$

Emcee has this approximation built in and we use it for further calculations. We expect the autocorrelation time to depend on the geometry we sample in and the magnetic field we use. We discuss three simple geometries: a square, a rectangle and a circle. For each geometry we inspect the autocorrelation time for an ensemble of a thousand walkers with a burn-in period of 1000 iterations.[11] The starting positions of the chains are picked uniformly in angle-position space. We evolve the chains until we have 20,000 independent samples in total per field. This is enough to quantitatively compare the current between fields.

[11] This allows the Markov chains to find modes of the distribution and so prevents biasing due to the starting positions.

Square

We start out with a simple geometry: a square of 2 μm by 2 μm. There is one obvious mode which results in a valid Andreev state, namely a trajectory with cyclotron radius equal to half of the sides which leaves the first superconducting contact in the center at a right angle (see figure 4.3). This trajectory is entirely symmetric so dependencies on k_F drop out.

There are other modes: if the length of the side walls is an integer multiple of the cyclotron diameter we have at least one Andreev bound state. When $R = 1/n$ the length of the total trajectory of a bound state is the sum of the corner circle segments and the side circle segments:

$$l = 4(n-1) \cdot \pi R + 4\frac{\pi}{2}R = 2\pi\frac{2n-1}{n}.$$

The shortest trajectory is the same trajectory as the one shown in 4.3. Due to exponential decay of the acceptance chance as a function of the trajectory length this is the mode we expect to yield the highest current.

The autocorrelation for this mode drops quickly in the beginning for both the angle and the position; see figure 4.4. Afterwards there is a long period of oscillatory behaviour which settles down after about 800 steps. To be on the safe side we take a step interval of a 1000 to guarantee independent samples. We evolve each chain for 21,000 steps to satisfy our desired sample amount.

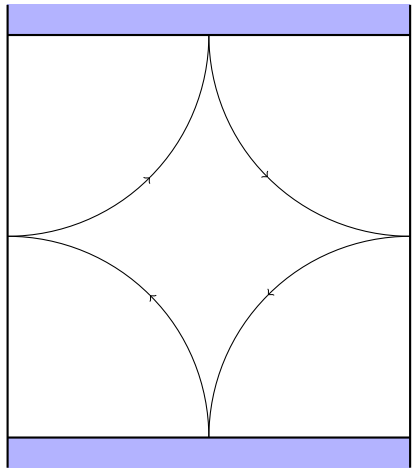

Figure 4.3: A square Josephson junction with its primary mode. An electron with a cyclotron radius equal to half of the sides of the square makes a perfect loop.

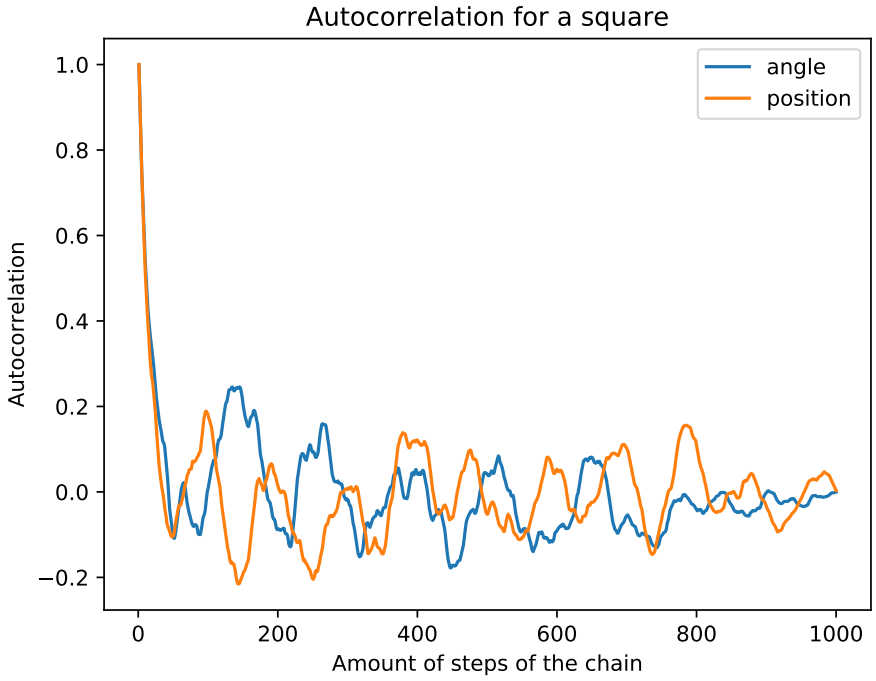

Figure 4.4: The autocorrelation of a Markov chain in a square geometry as a function of the interval between instances. The autocorrelation fluctuates with an approximately constant frequency with a noticeable decay after 800 steps.

Rectangle

The second basic geometry we look at is a rectangle with a contact width of 1 μm and a length of 2 μm. We show two possible modes for Andreev states in figure 4.5. It behaves very similarly to the square junction in this aspect in that these modes become more unlikely as the curvature increases. The main difference is the magnetic field at which a mode forms. By lowering the width of the geometry we lower the field required to get a mode. If we were able to adjust the width while measuring we could find the field this way!

Sadly this is not realistically possible. What is possible is calculating the autocorrelation of a single Markov chain for the resonance mode of the geometry: figure 4.6. The autocorrelation for this chain dies out more quickly than for the square geometry. This is entirely reasonable; different chains explore different parts of position-angle space. For this chain 600 steps is sufficient for quasi-independence. To prevent arbitrariness per geometry we use the same settings as for the square geometry: 1000 steps per sample.

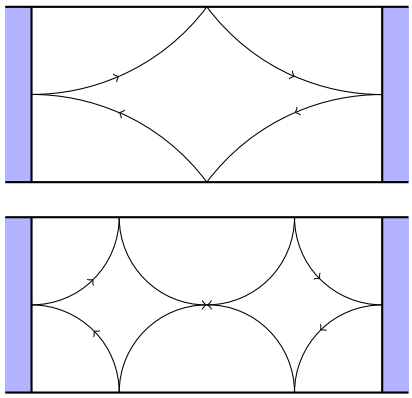

Figure 4.5: Two possibilities for Andreev modes in a rectangular junction of 2 by 1 μm. The trajectory with the least curvature is the shorter and as such more likely to carry current.

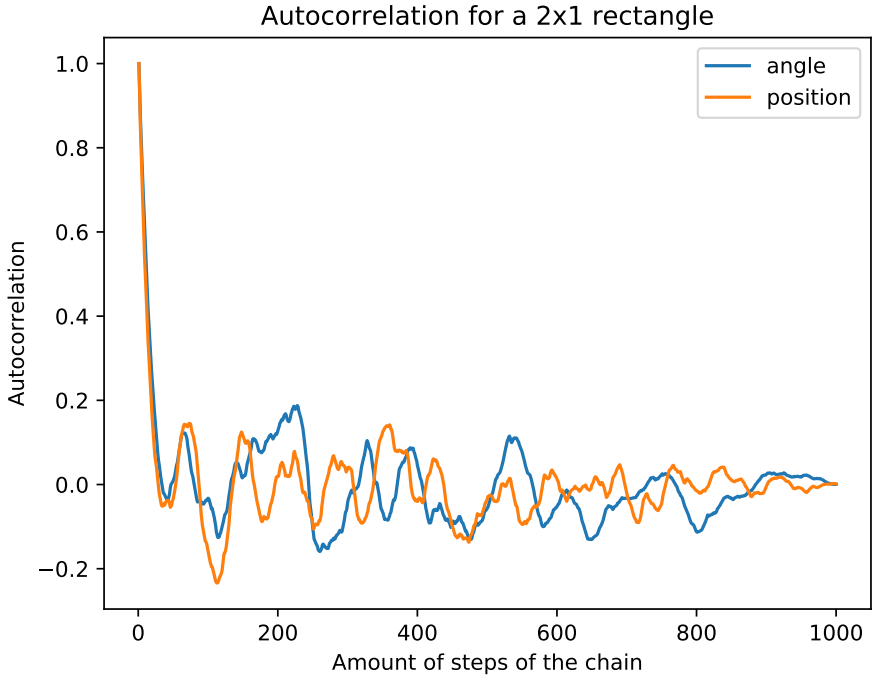

Figure 4.6: The autocorrelation for a Markov chain in a 2x1 rectangular geometry. We judge 600 steps enough to speak of independent samples for this chain.

Circle

The last geometry we discuss is the most interesting one: a circular geometry. It allows for the same modes as the square geometry when the cyclotron radius is equal to the geometry radius (see figure 4.7). The advantage of the circle geometry is that

this mode is orientation independent. We can start from anywhere on the contact and get a closed loop if the trajectory starts out paraxial to the contact. Since we have more modes than in the square geometry we also expect a greater current given that the modes do not interfere destructively.

At least that is how it would seem. In fact the circle geometry supports significantly more modes. All trajectories that hit the side walls once or not at all before arriving at the second superconducting contact form an Andreev bound state! Due to symmetry any reflection of the electron trajectory will be mirrored by the hole trajectory in respect to the center of the circle geometry (see figure 4.8). This mirroring fails when a trajectory hits the same superconducting contact twice. We get well defined areas where there are no Andreev bound states and areas where everything is an Andreev bound state.

This characteristic complicates the sampling. In the square and rectangle geometries the allowed states are very close to each other so the phase does not fluctuate a lot. For the circle geometry we have a larger area to sample so we need significantly more samples. We obtain these samples not with MCMC but with regular uniform sampling. Since almost all trajectories are valid close to the resonance field we do not need a sniper where a shotgun suffices. We use a tenfold compared to other geometries: 200,000 samples per field.

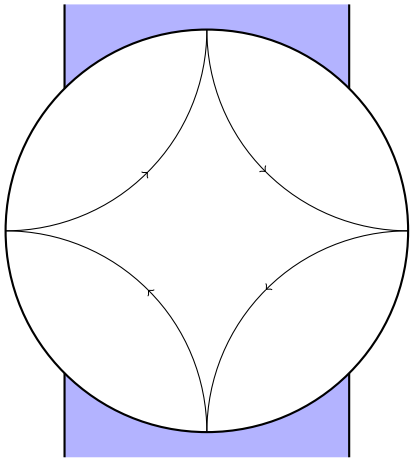

Figure 4.7: A circular Josephson junction with its most obvious mode for a cyclotron radius equal to the geometry radius. In fact all trajectories that hit both side walls once form a valid trajectory.

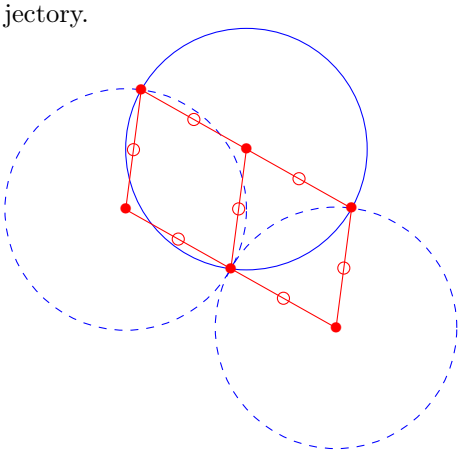

Figure 4.8: The left dashed circle represents an electron going out and the right dashed circle represents a hole coming in at the same angle and position. The line connecting the intersections goes through the center of the circle geometry allowing for rotational symmetry. The whole trajectory forms a perfect Andreev state.

4.6 Conclusion

We are all set to actually sample the geometries and calculate the appropriate currents. If we can prove that currents exist in high fields for these geometries we can build composite geometries. If well executed the combined geometry sustains most modes belonging to the basic geometries we have discussed. Together these modes give regular peaks in current at certain magnetic field intervals: exactly what we are looking for.

References

[1] Luca Banszerus et al. “Ballistic transport exceeding 28 μm in CVD grown graphene”. In: *Nano Lett.* 16.2 (2016).

[2] S. Behnel et al. “Cython: The Best of Both Worlds”. In: *Comput Sci Eng* 13.2 (2011).

[3] A. H. Castro Neto et al. “The electronic properties of graphene”. In: *Rev. Mod. Phys.* 81.1 (2009).

[4] Hidde Dijkstra. “Uniform magnetic field raytracer and sampler”. In: (2018). DOI: 10.5281/zenodo.1197515.

[5] Daniel Foreman-Mackey et al. “emcee: The MCMC Hammer”. In: *PASP* 125.925 (2013).

[6] Charles Kittel. *Introduction to Solid State Physics*. 5th. New York: John Wiley & Sons, Inc, 1976.

Results & discussion

The inclusion of the Fermi wavevector to the complex phase difference $\Delta\phi$ results in chaotic systems. We drop this quantity in favor of studying the Aharonov-Bohm phase. This phase is non-chaotic or integrable when the trajectories that make up the mode only reflect at right angles. For rectangles with dimensions with an integer ratio these modes exist and allow a current for a small range of fluxes. Within this range the Josephson current changes shape. We propose that this shape allows us to pinpoint the magnetic field strength.

5.1 Introduction

It is time to actually start sampling the different geometries and calculate the currents. Before we go to the results we have to start with a disclaimer. We have found that the Fermi wavevector dependency of the phase $\Delta\phi$ adds a significant amount of chaos to the system. Every 10 nm (the Fermi wavelength) that the hole and electron trajectory lengths differ adds 2π to the phase. A small change in the beginning conditions can easily amount to length differences of more than 50 nm in systems with length scales of 1 μm. This makes high field geometries highly chaotic and reduces any numerical calculations of the current to pure noise.

Luckily all is not lost; the Aharonov-Bohm phase is integreable. The main modes are symmetrical so the dependence on the Fermi wavevector drops out in a small neighbourhood. If the drop in current as a result of chaos is comparable for all magnetic fields we can still calculate relative currents. In the results we do not express the currents in quantitative units. Without considering k_F any quantitative value is meaningless.

We discuss the geometries in the same order as in the implementation chapter. First we look at the location of Andreev states in position-angle space. The position takes values in a range of 0 to 1 in respect to the superconducting contact with 0.5 the center of the contact. The angle takes values from 0 to π with $\pi/2$ indicating a trajectory that leaves the contact at a right angle. Each Andreev state has an associated Aharonov-Bohm phase between 0 and 2π. We use a periodical color scheme to signify the phase in the results.

Depending on the interference pattern in the Aharanov-Bohm phases we find a Jospehson current. In small field junctions this current is approximately a sine of the superconducting phase difference between the contacts. When this phase difference is

zero we expect no current to flow between the contacts. The level at which the current satisfies these properties gives a measure for the amount of statistical noise.

Next we compare the maximal currents per field in a neighbourhood. It is at this point that extended bridge sampling comes into play. The Josephson current plots only show how well the Aharonov-Bohm phases align: the smaller the current, the greater the destructive interference between Andreev states. These plots do not take in account the probability of states; they only show which states are more probable in this specific situation. Using the normalization constants provided by extended bridge sampling we achieve a qualitative picture of the critical current (maximal current) as a function of the magnetic field.

5.2 Square

A square geometry of 2 μm by 2 μm has its main mode when the cyclotron radius is equal to half of the side length. Accordingly we expect the current to peak at 800 Φ_0 (flux quanta) as shown in figure 5.1. We have sampled 50 values in total around this expected peak value. In figures 5.2a-5.2h we show how the interference patterns develops for fluxes in the neighbourhood of the resonance. At the peak value of 800 Φ_0 there is a large area of constant phase around the main mode. For the other plots the destructive interference is greater since the oscillations at the fringes penetrate further inward.

The Josephson currents between 790 and 810 Φ_0 are continuous and resemble sine functions to some degree. At superconducting phase differences of 0, π and 2π the current is zero as we predicted. For fluxes greater than 820 Φ_0 the sinusoidal relation breaks down because new states start appearing. These new states live in the corners of the geometry where they make multiple small bounces along the side walls to reach the other contact. The current contribution from these states create the noise in figure 5.2h.

The unnormalized current peaks at a flux slightly larger than the predicted 800 (see figure 5.3). On the other hand the relative normalization peaks at a flux smaller than 800 Φ_0. Combining the two does result in a current peak close to the expected value. Figures 5.2a-5.2h explain this competition. For lower fields the area of allowed states is larger resulting in a larger relative normalization while for higher fields the fringes disappear: removing sources of destructive interference. The optimum lies somewhere in between; just under 800 Φ_0.

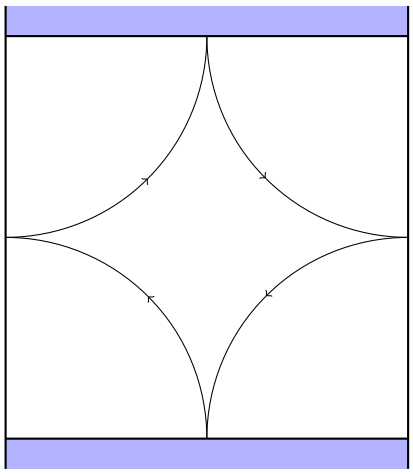

Figure 5.1: The mode in a square geometry: the trajectory leaves the contact from the center at a right angle.

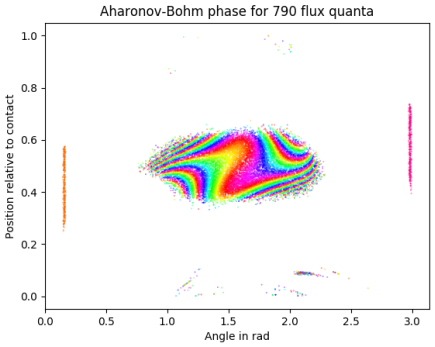

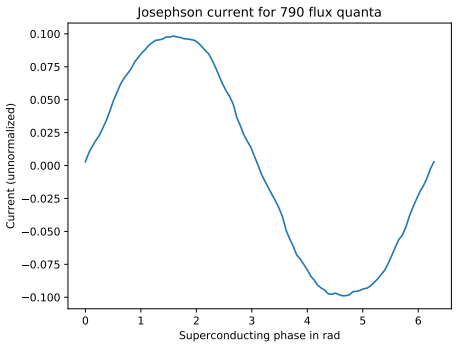

Figure 5.2(a): The Aharonov-Bohm interference pattern in a square junction for a flux of 790 Φ_0. On the sides there are two lines with constant phase. These do not contribute to the current since the trajectory velocities close to 0 and π are perpendicular to the superconducting contact.

Figure 5.2(b): The Josephson current in a square junction for a flux of 790 Φ_0. The Josephson current is approximately sinusoidal as expected. Its zeros are correctly predicted as 0, π, and 2π.

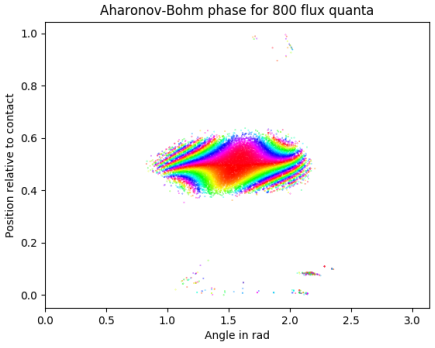

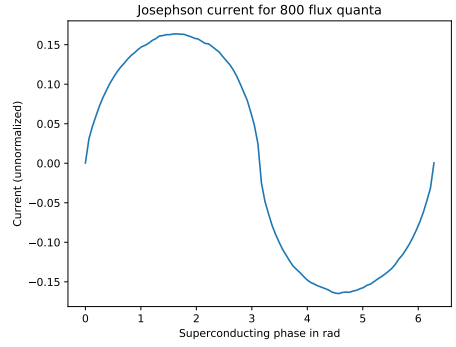

Figure 5.2(c): The Aharonov-Bohm interference pattern in a square junction for a flux of 800 Φ_0. The center (in red) is constant and relatively large compared to the fringes. We expect the oscillations in the fringes to interfere destructively; allowing the center to carry a current.

Figure 5.2(d): The Josephson current in a square junction for a flux of 800 Φ_0. Instead of resembling a sine it has characteristics of a block function: it changes rapidly at the turning points to remain relatively constant in between.

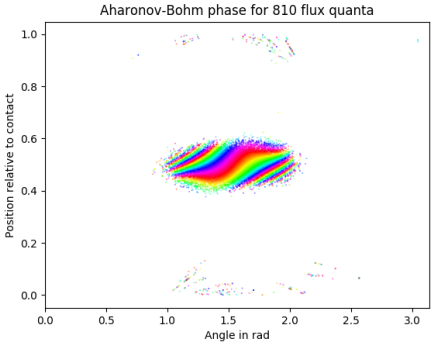

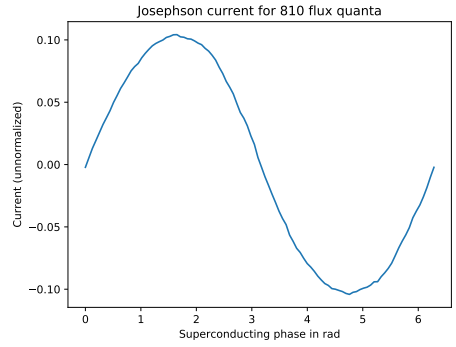

Figure 5.2(e): The Aharonov-Bohm interference pattern in a square junction for a flux of 810 Φ_0. The interference pattern resembles a smaller, mirrored version of the Aharonov-Bohm phase for 790 Φ_0.

Figure 5.2(f): The Josephson current in a square junction for a flux of 810 Φ_0.

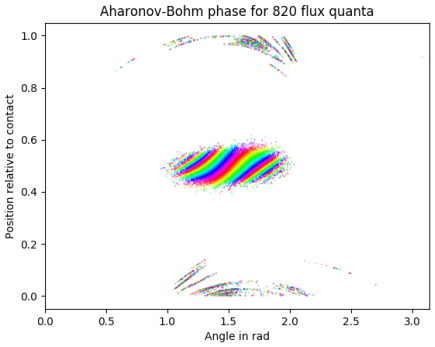

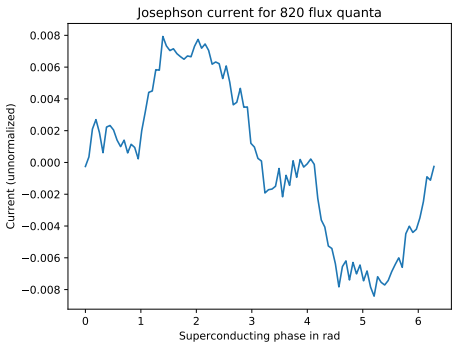

Figure 5.2(g): The Aharonov-Bohm interference pattern in a square junction for a flux of 820 Φ_0. At the corners of the geometry new states start appearing. These correspond to trajectories which walk quasi-linearly along the side walls to make a large circular move back to the origin.

Figure 5.2(h): The Josephson current in a square junction for a flux of 820 Φ_0. The new states appearing in the corners interfere with the sinusoidal pattern creating a significant amount of noise.

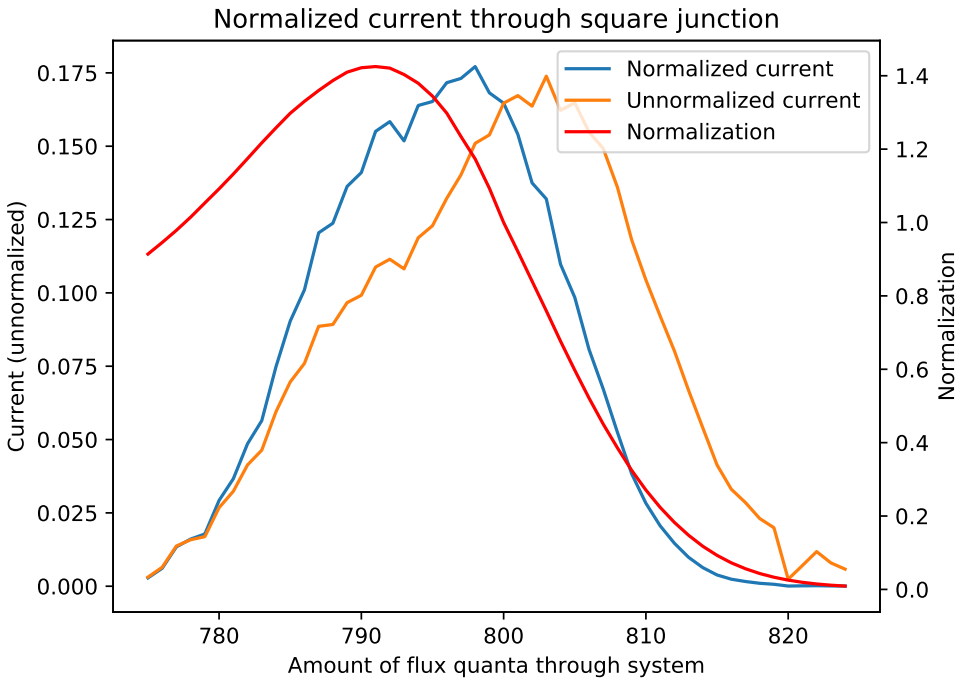

Figure 5.3: The critical current in a square junction for flux values close to the resonance flux of 800 Φ_0. For a square junction resonance effects appear when the cyclotron radius is equal to half of the side wall length. The competition between normalization and constructive interference results in a current peak slightly below the expected resonance value of 800 Φ_0.

5.3 Rectangle

Our second geometry is similar to our first. A square is just a special case of a rectangle so we expect similar modes. Our rectangle has superconducting contact lengths of 1 μm and side walls of 2 μm. We look for equivalent modes to the mode we discovered in the square geometry. We have two ways of interpreting the mode:

1. The square resonates when trajectories reflect from the middle of the side walls. The electron and hole trajectories are perfectly symmetric and cover the minimal amount of distance. We call this mode the "Single bounce mode".

2. The square resonates when trajectories reflect at 90°. This restricts the allowed dimensions of a rectangle geometry to integer ratios. For a 2x1 rectangle this requires two bounces on the side walls. We call this the "Double bounce mode".

Single bounce mode

The first mode takes place for a cyclotron radius of 4/5 of half of the side wall length. The field strength required is equivalent to a flux of 320 Φ_0.[12] Figures 5.6a-5.6g show the Andreev states centered around the same mode as for the square geometry. The shape of the interference region differs however in orientation and structure. Depending on the sign of the magnetic field the region has a diagonal inclination. The constant

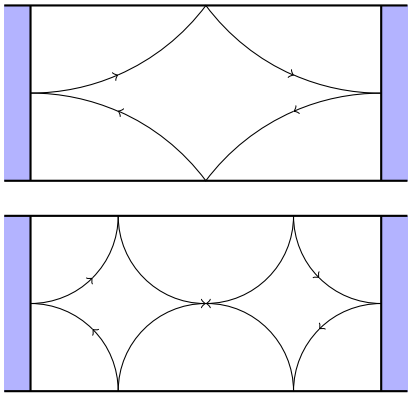

Figure 5.4: The two modes for a rectangular junction: the single bounce and the double bounce.

[12]The area of the rectangle is half of that of the square so the amount of enclosed flux quanta is halved.

phase region in the center of the interference region is also absent. Trajectories around the main mode interfere destructively allowing small regions in the periphery to dominate any current. These peripheral regions are prone to biased sampling since Markov chains can easily get stuck.

We see the absence of a main current source in the Josephson currents as well. There is an overall tendency to a triangular dependency on the superconducting phase. Noise dominates however; any current that is present is small compared to the current in the square geometry. This susceptibility to noise results from the reflection at the side walls. Reflections at 90° are resilient when it comes to small perturbations of the starting angle or position. For the rectangle the reflection angle is approximately 50° which compresses the region of constant phase in the center of the interference region until it is indiscernible from the fringes.

The critical currents as plotted in figure 5.5 confirm our suspicions. There is no trace of a pattern or structure in the current, whether normalized or unnormalized. The normalization does have a clear preference for the expected mode at 320 Φ_0. If there is a current peak at all then the normalization is the source of it. This geometry does not fit our needs: there is no response currentwise for any flux in the range of 300-340 Φ_0.

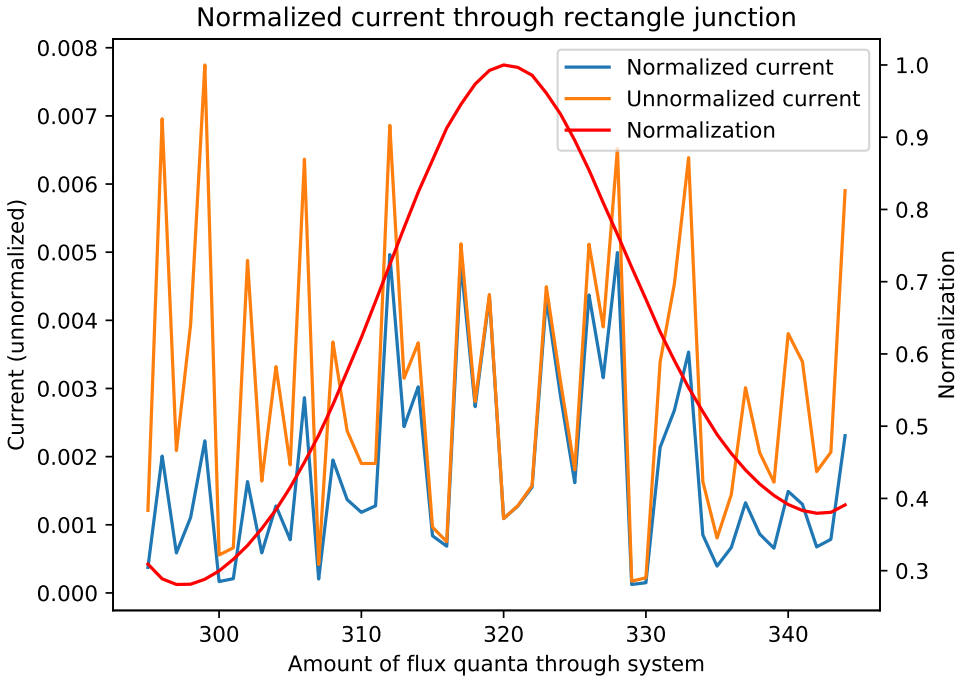

Figure 5.5: The critical current in a rectangular junction for values of the flux close to the expected resonance flux of 320 Φ_0. The expected resonance is absent since there is no constant phase region.

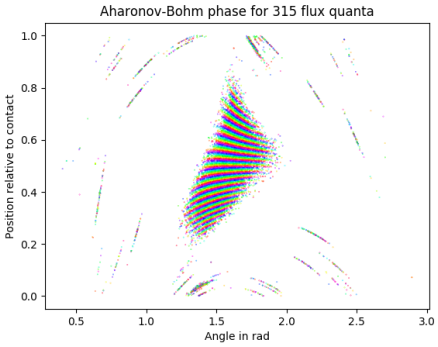

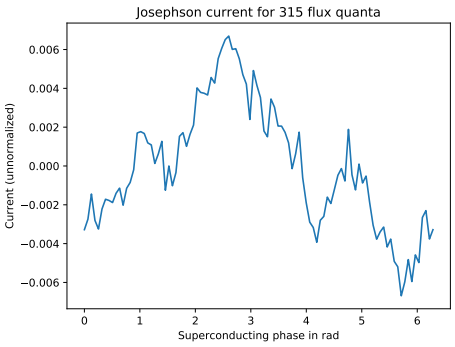

Figure 5.6(a): The Aharonov-Bohm interference pattern in a rectangular junction for a flux of 315 Φ_0. There is no region of constant phase so destructive interference dominates.

Figure 5.6(b): The Josephson current in a rectangular junction for a flux of 315 Φ_0. It tends to follow a triangular relation to the superconducting phase.

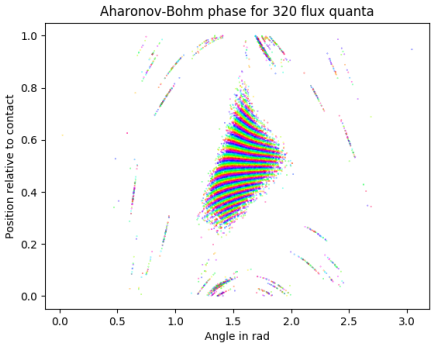

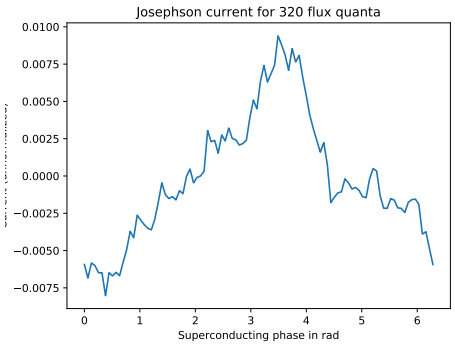

Figure 5.6(c): The Aharonov-Bohm interference pattern in a rectangular junction for a flux of 320 Φ_0.

Figure 5.6(d): The Josephson current in a rectangular junction for a flux of 320 Φ_0.

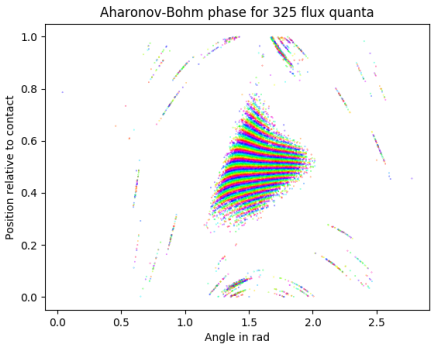

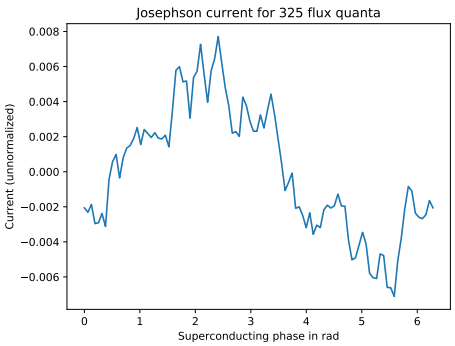

Figure 5.6(e): The Aharonov-Bohm interference pattern in a rectangular junction for a flux of 325 Φ_0.

Figure 5.6(f): The Josephson current in a rectangular junction for a flux of 325 Φ_0.

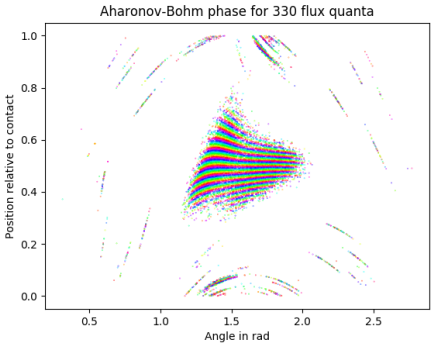

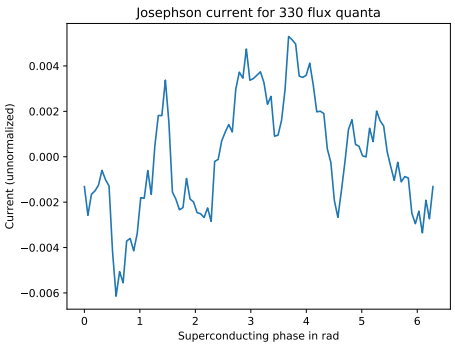

Figure 5.6(g): The Aharonov-Bohm interference pattern in a rectangular junction for a flux of 330 Φ_0. There is an interesting development in the interference region. It is splitting in two regions: one moving to the right and one moving to the left. For higher fields this development results in new modes.

Figure 5.6(h): The Josephson current in a rectangular junction for a flux of 330 Φ_0. The noise has increased to such a degree that the current has even lost any resemblance to a triangular pattern.

Double bounce mode

The single bounce mode floundered due to its acute reflection angles. The double bounce mode on the other hand consists purely of reflections at right angles. These trajectories are more stable and hopefully carry a current.

In figures 5.8a-5.8h we have once more plotted the Aharonov-Bohm interference patterns and the Josephson currents. Both the interference patterns and the currents are familiar. They are nearly identical to the square geometry! For this mode a rectangle is equivalent to lining up two square junctions. All trajectories pass through the center so they enter the second square from an identical configuration of positions and angles as required for a single square. As a result the normalization for the rectangle junction has the same shape as for the square junction. Since this mode requires a higher field strength the current peak is narrower (see figure 5.7).

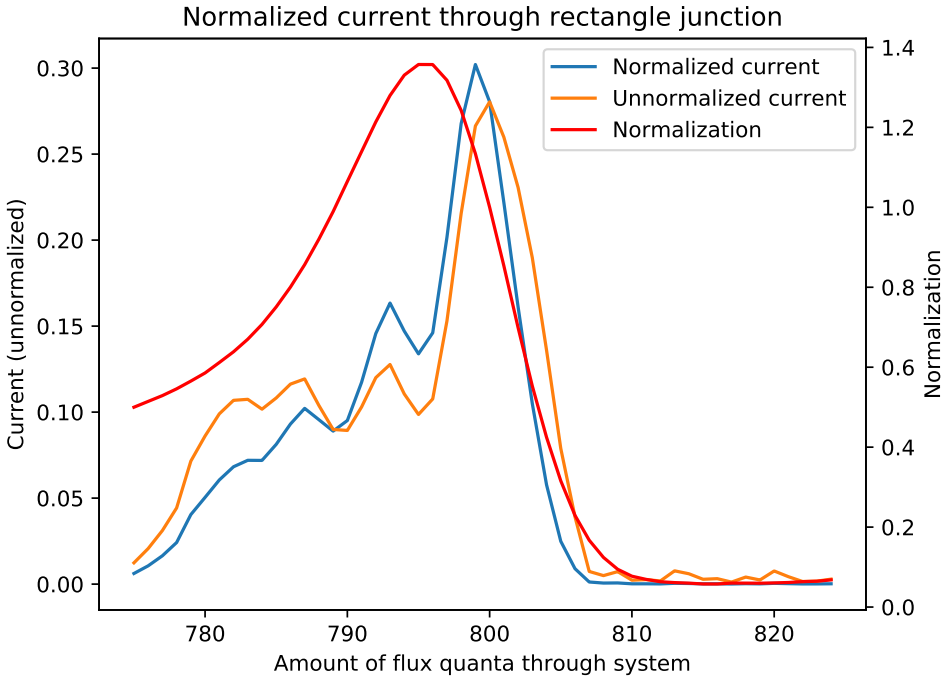

Figure 5.7: The critical current in a rectangular junction as a function of the flux. There is a sharp peak at a flux of 795-803 Φ_0 with a more gradual decay for smaller values of the flux.

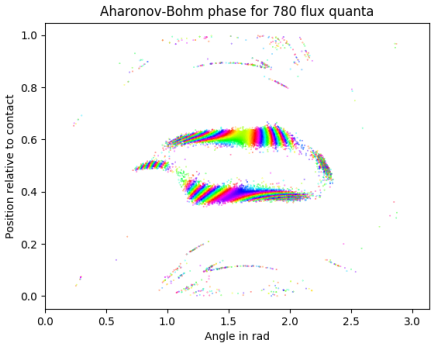

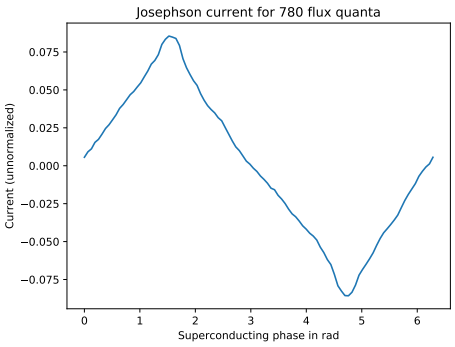

Figure 5.8(a): The Aharonov-Bohm interference pattern in a rectangular junction for a flux of 780 Φ_0. The regions have oscillatory 'wings' which interfere destructively. The centers are relatively constant and result in a non-zero current.
Figure 5.8(b): The Josephson current in a rectangular junction for a flux of 780 Φ_0. The shape follows a near perfect triangular pattern. It obeys the expected zeros at the phase differences 0, π, and 2π.

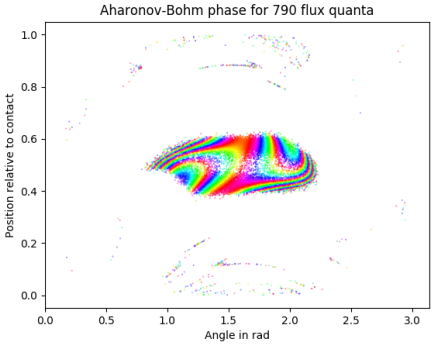

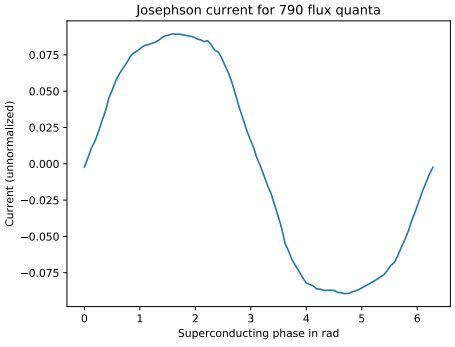

Figure 5.8(c): The Aharonov-Bohm interference pattern in a rectangular junction for a flux of 790 Φ_0. The regions are joining together into a pattern reminiscent of the pattern in figure 5.2a.

Figure 5.8(d): The Josephson current in a rectangular junction for a flux of 790 Φ_0. The shape is somewhere in between a rectangular and sinusoidal pattern.

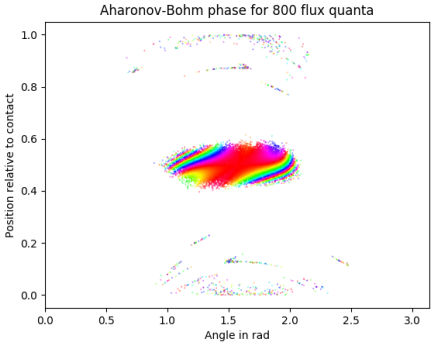

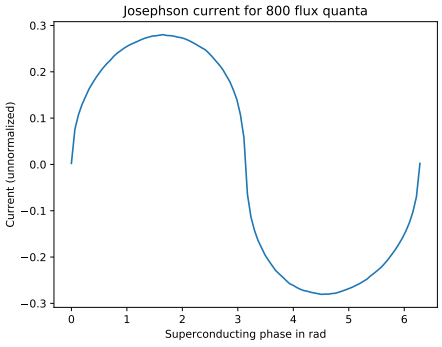

Figure 5.8(e): The Aharonov-Bohm interference pattern in a rectangular junction for a flux of 800 Φ_0. Similarly to figure 5.2c we find a large area of constant phase in the center. There are however less oscillations at the fringes: less sources of destructive interference.
Figure 5.8(f): The Josephson current in a rectangular junction for a flux of 800 Φ_0. The current rises steeply from its zeros and has a relatively constant maximum. We have seen this before for the square junction (see figure 5.2d).

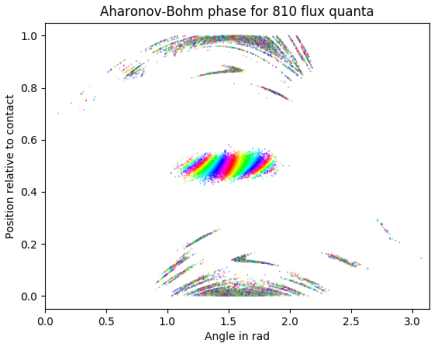

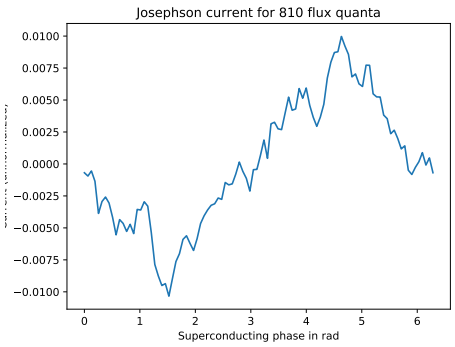

Figure 5.8(g): The Aharonov-Bohm interference pattern in a rectangular junction for a flux of 810 Φ_0. The corner modes are sucking the center mode dry; their noise obscures current through the junction.

Figure 5.8(h): The Josephson current in a rectangular junction for a flux of 810 Φ_0. The overarching structure is triangular and obeys the expected zeros.

5.4 Circle

The last geometry we study is the circular junction. For the resonance field such that the cyclotron radius is equal to the geometry radius almost all trajectories are valid Andreev states. We sample the trajectories uniformly instead of biasing with MCMC. Due to the absence of biasing we do not need to normalize the currents relatively. Quantitative normalization is still impossible: we still disregard k_F.

The Aharonov-Bohm phase also offers extra trouble for the circular geometry. In our gauge the integral over the contact is non-zero: the superconducting phase is variable. We have corrected for this deficiency in figures 5.11a-5.11h. Depending on where we choose our reference point the areas of constant phase move. We have picked the middle of the contact as the reference point and include the integral over the contact in the Aharonov-Bohm phase of the trajectory.

The interference plots show two regions of constant phase. Each belongs to one of the modes in figure 5.9. The two are not necessarily in phase; in figure 5.11h they successfully work together to reduce the Josephson current to zero for most superconducting phase differences. The advantage of having two constant phase areas shows itself in figure 5.10. The critical current shows oscillatory behavior as a function of the flux.

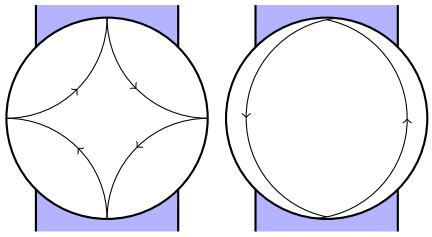

Figure 5.9: The two modes in the circle junction. The first one reflects once off each side wall and leaves the contact at a right angle. The second Andreev reflects twice at each contact but leaves the contact at a sharp angle, reducing its current contribution.

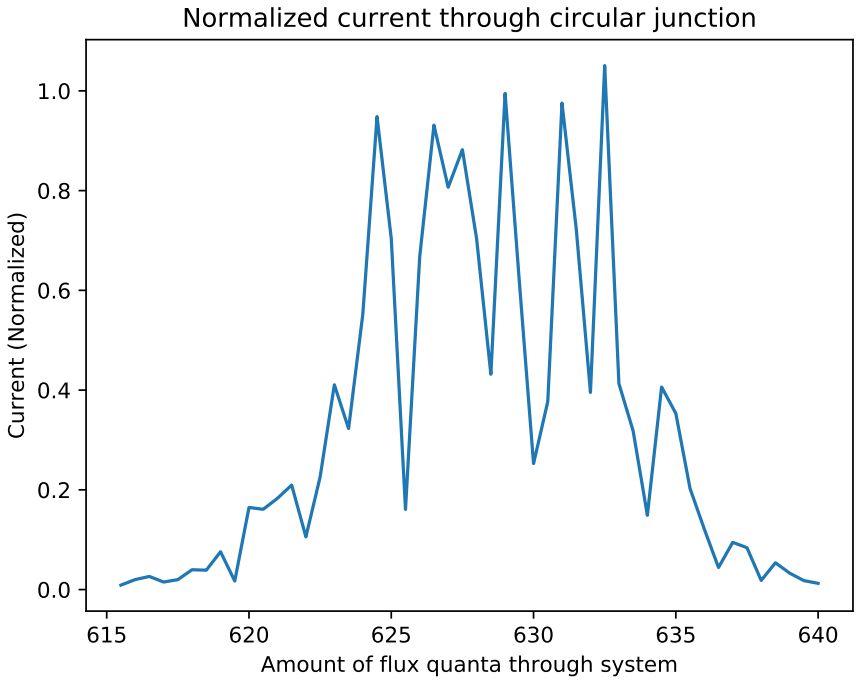

Figure 5.10: The critical current in a circular junction as a function of the flux. There is oscillatory behavior due to interference effects between two areas of constant phase in the Aharonov-Bohm interference patterns.

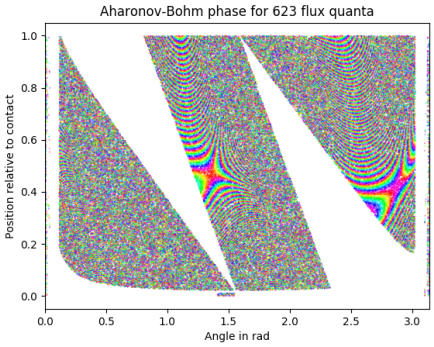

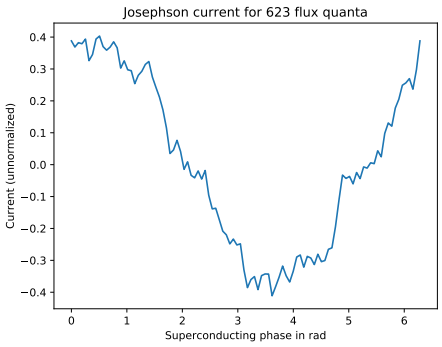

Figure 5.11(a): The Aharonov-Bohm interference pattern in a circular junction for a flux of 623 Φ_0. There are two 'Bermuda triangles' where even uniform samples scare away from. There are two centers of constant phase which interfere with each other.

Figure 5.11(b): The Josephson current in a circular junction for a flux of 623 Φ_0. Our gauge choice shifts the superconducting phase difference: the zeros of the current are not at 0, π, and 2π.

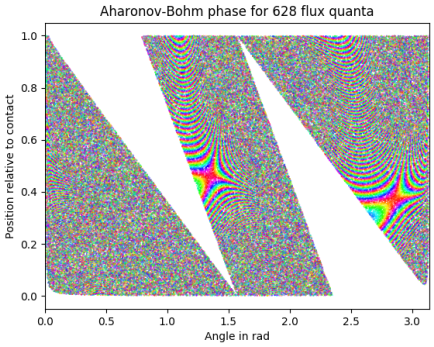

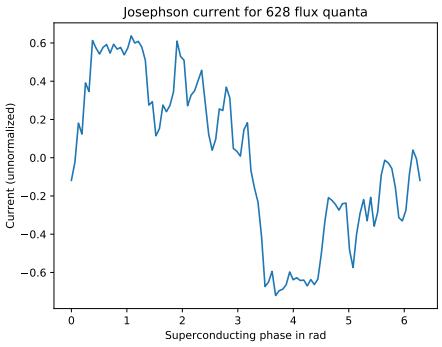

Figure 5.11(c): The Aharonov-Bohm interference pattern in a circular junction for a flux of 628 Φ_0. We recognize this as the resonance mode; all states besides the forbidden triangles are occupied by samples. The two constant phase areas interfere constructively.

Figure 5.11(d): The Josephson current in a circular junction for a flux of 628 Φ_0.

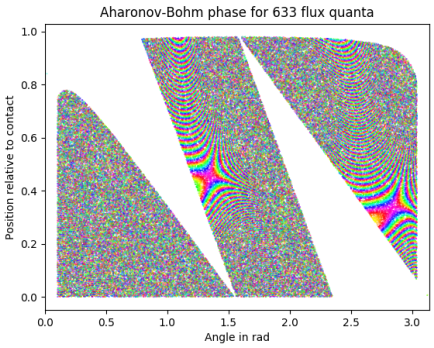

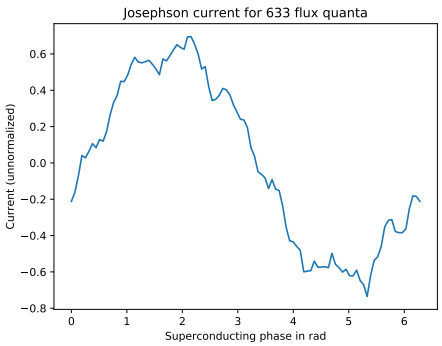

Figure 5.11(e): The Aharonov-Bohm interference pattern in a circular junction for a flux of 633 Φ_0.

Figure 5.11(f): The Josephson current in a circular junction for a flux of 633 Φ_0.

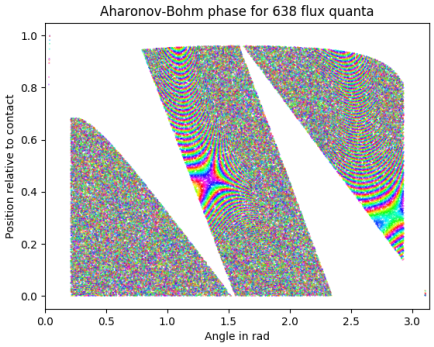

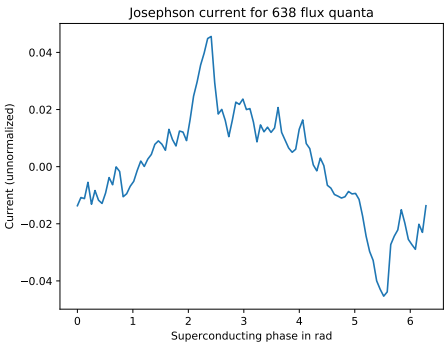

Figure 5.11(g): The Aharonov-Bohm interference pattern in a circular junction for a flux of 638 Φ_0. The phase centers interfere destructively.

Figure 5.11(h): The Josephson current in a circular junction for a flux of 638 Φ_0. The destructive interference reduces the current to noise around zero with two peaks.

5.5 Discussion

In 1962 Brian David Josephson found a physical explanation for a slightly unusual phenomenon: a finite current between two superconductors separated by a thin insulator. Can we say the same now for two superconductors separated by a larger geometry at high magnetic fields? The answer we give is: well... maybe... sometimes.

'Sometimes' adheres to strict conditions on both the field and the geometry. Current only flows close to resonance fields of the geometry. Trajectories that contribute to current must reflect at right angles, independent of geometry. This limits possible geometries to the basics: polygons with congruent angles and circles. The cyclotron radius of the desired resonance field must fit an integer number of times in each vertice of the polygon to get a closed trajectory.

The challenge lies in choosing a geometry that destroys all modes that disturb our main resonance modes. The circular junction fails in this regard and has noisy Josephson currents due to the plethora of modes it sustains. The advantage the circular junction has is its two modes which interfere with each other. Unlike the rectangular geometries the circle has a clear oscillation in its critical current. If we squint really hard we might even think to recognize a Fraunhofer pattern. Whether this oscillation survives in the real world is not clear. Nevertheless, we are confident that there is a current at the resonance field.

The second geometry of interest is the two by one rectangle. Compared to the square the greater precision required for two successful bounces reduces the oscillation in the fringes. We recognize this absence of interference in the crisp Josephson current. From a triangular signal it gradually develops into a block like pulse. This pulse is the current for a junction with constant Aharonov-Bohm phase:

$$I \propto \frac{\sigma(\tilde{\epsilon})\sqrt{1-\tilde{\epsilon}^2}}{1+\sqrt{1-\tilde{\epsilon}^2}}, \tag{5.1}$$

with $\tilde{\epsilon}$ depending linearly on the superconducting phase difference.

Because we have neglected values for $\tilde{\epsilon}$ larger than one the Josephson currents are not perfectly symmetrical. Near the values 0 and 2π we lose signal. This asymmetry is small and we conclude that our simplification has not altered our results to a great degree.

By integrating the current and dividing by the critical current we get a measure of how 'round' the Josephson current is. We have an analytical expression for both a traingular signal and the resonance signal. Intrapolating for fluxes in between gives us a measure 'roundness' in terms of flux. As such we can 'measure' the field strength by integrating the current in a real life set up.

A second possibility is artificially creating a second mode. We do this by attaching another rectangular junction to the superconducting contacts but with slightly different dimensions. If the second rectangle has vertices slightly smaller than the first its resonance field is slightly higher. For the same field trajectories in both junctions acquire slightly different complex phases and interfere with each other. The oscillations in the critical current then indicate the in plane field. We do not suffer the same amount of noise as for the circle. The geometry silences all but the two resonance modes.

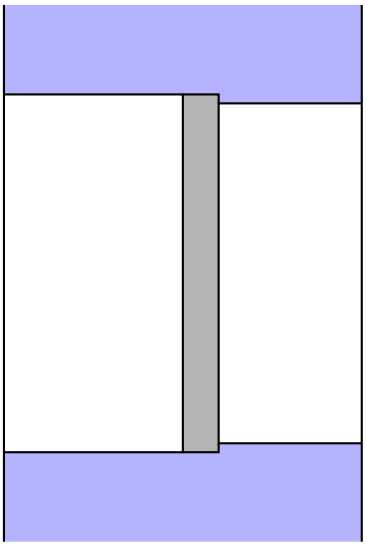

Figure 5.12: A junction consisting of two rectangular geometries with slightly different dimensions. The modes evolve differently as a function of the field creating an interference effect between the two.

5.6 Conclusion

We have successfully implemented the MCMC sampler emcee to acquire the Andreev states in a square, rectangular, and circular junction. These states form Aharonov-Bohm interference patterns in position-angle space. Depending on the area of constant phase a Josephson current flows through the junction. We suggest experimentally measuring the shape of the Josephson junctions in a rectangular geometry near the resonance field. It is here that we expect the transition of the Josephson current from a triangular pulse to a circular-rectangular one.

Conclusion and outlook

We set out to find geometries which support supercurrent between two contacts at high uniform magnetic fields. At these fields we cannot neglect the curvature of electron and hole trajectories. As such we have reexamined the existing theory and supplemented it to accommodate circular trajectories. We find that circular trajectories have strict requirements for carrying current. Electron and hole trajectories must form a loop to form an Andreev bound state.

Here lies the difficulty in calculating currents flowing through a junction. We have no explicit equation which tells us whether a trajectory is an Andreev bound state or not. For most fields and geometries these states are rare and difficult to find. For this purpose we formulate the chance of accepting a trajectory as an unnormalized probability distribution. This formulation allows us to use statistical tools in estimating the current.

We opt to use a Monte Carlo approach which uses Markov chains to sample probability distributions. The Python package emcee supplies a specialized variant of Markov chain Monte Carlo sampling called the stretch move method. It uses an ensemble of Markov chains to predict the curvature of a probability distribution. The stretch move lowers the autocorrelation time of sampling by aligning the step with the curvature.

We collect samples of Andreev states for different fluxes to estimate the critical current as a function of the magnetic flux. For circular, rectangular and square geometries we find resonance effects around fields for which the cyclotron radius fits an integer number of times in the geometrical length scales. An important requirement for stability in the resonance is that trajectories reflect at right angles. At acute reflection angles small differences in starting conditions result in rapid oscillatory behavior in the Aharonov-Bohm phase. These combinations of geometries and fields are chaotic and do not support a current.

Of the geometries that do support resonance modes we recognize the rectangular geometry as the most stable. Multiple bounces at right angles supress large deviations from the resonance mode and the highly oscillatory phase they carry. The Aharonov-Bohm interference pattern is constant and the Josephson current behaves according to an analytical expression. We suggest relating the shape of the Josephson current to the flux. Integrating the current then gives an accurate estimate of the applied field.

We recognize the need to verify the existence of resonance modes at high fields experimentally. If confirmative we propose combining rectangular junctions of slightly different sizes to create interference patterns in the supercurrent.

Appendix

7.1 WKB approximation

The WKB approximation has its very imaginative name because it was developed by Wentzel, Kramers, and Brillouin. It tries to remove the highest derivative of a differential equation when the highest derivative has a small forefactor ε. In quantum mechanics this role is reserved for $\hbar$. We attempt a similar method by splitting the solution to the wave equation ψ in an oscilatory and an amplitudal part. Higher derivatives in the amplitudal part do not survive the semi-classical limit of $\hbar \to 0$.

The Bogoliubov-de Gennes equations in the absence of an electric field are:

$$-\frac{\hbar^2}{2m}\left(\nabla - \frac{ie}{\hbar}\mathbf{A}\right)^2 u - \mu + \Delta v = eU$$
$$\frac{\hbar^2}{2m}\left(\nabla + \frac{ie}{\hbar}\mathbf{A}\right)^2 v - \mu + \Delta^* u = eV$$

We use the substitution as given in equation 2.6:

$$\begin{pmatrix} u \\ v \end{pmatrix} = \mathrm{e}^{i\phi_e(\mathbf{r})}\begin{pmatrix} U(\mathbf{r}) \\ 0 \end{pmatrix} + \mathrm{e}^{i\phi_h(\mathbf{r})}\begin{pmatrix} 0 \\ V(\mathbf{r}) \end{pmatrix}.$$

with $|\mathbf{k}| = k_F$.

We derive the first Andreev equation for U. The derivation for V is identical save for the particle charge. The first derivative is:

$$\begin{aligned}\left(\nabla - \frac{ie}{\hbar}\mathbf{A}\right) u &= iu\nabla\phi_e + \mathrm{e}^{i\phi_e}\nabla U - \frac{ie}{\hbar}\mathbf{A}u \\ &= u\left(i\mathbf{k} + \frac{ie}{\hbar}\mathbf{A}\right) + \mathrm{e}^{i\phi_e}\nabla U - \frac{ie}{\hbar}\mathbf{A}u \\ &= i\mathbf{k}u + \mathrm{e}^{i\phi_e}\nabla U,\end{aligned}$$

the magnetic vector potential drops out. The second derivative is:

$$\begin{aligned}\left(\nabla - \frac{ie}{\hbar}\mathbf{A}\right)^2 u &= i\mathbf{k}(i\mathbf{k}u + \mathrm{e}^{i\phi_e}\nabla U) + \left(\nabla - \frac{ie}{\hbar}\mathbf{A}\right)\mathrm{e}^{i\phi_e}\nabla U \\ &= -\mathrm{e}^{i\phi_e}(|\mathbf{k}|^2 U + \mathbf{k}\cdot\nabla U) + \mathrm{e}^{i\phi_e}\left(\nabla^2 U + i[\nabla U][\nabla\phi_e] - \frac{ie}{\hbar}\mathbf{A}\nabla U\right) \\ &= \mathrm{e}^{i\phi_e}(k_F^2 U + 2\mathbf{k}\cdot\nabla U + \nabla^2 U).\end{aligned}$$

Conveniently the Bogoliubov-de Gennes equation also contains the chemical potential μ which is roughly equal to $k_F^2\hbar^2/2m$. This term cancels against the first term resulting from the second derivative. We substitute the derivatives into the equation:[1]

$$\begin{aligned}\epsilon U &= -\frac{\hbar^2}{2m}\mathrm{e}^{-i\phi_e}\left(\nabla - \frac{ie}{\hbar}\mathbf{A}\right)^2 u + \Delta V \mathrm{e}^{i\phi_h - i\phi_e} - \mu U \\ &= -\frac{\hbar^2}{2m}\nabla^2 U - i\hbar\mathbf{v}_F\cdot\nabla U + \Delta V\end{aligned}$$

We now apply the semi-classical approximation and drop the second derivative in U. This is the only term multiplied with $\hbar$ squared and as such negligible in semi-classical limit. The remaining equation is the first Andreev equation.

[1] For the right choice of gauge the magnetic vector potential is zero inside the superconductor so $\phi_e = \phi_h$ when $\Delta \neq 0$.

7.2 Extended bridge sampling

We start out using the estimator for the ratio as given by equation 3.6:

$$\frac{Z_2}{Z_1} \approx \frac{\frac{1}{n_1}\sum_{i=1}^{n_1}\alpha(\mathbf{x}_i^1)h_2(\mathbf{x}_i^1)}{\frac{1}{n_2}\sum_{j=1}^{n_2}\alpha(\mathbf{x}_j^2)h_1(\mathbf{x}_j^2)}.$$

This estimator becomes worse as the overlap between two probability distributions becomes small. We expect this to happen for $y_i = Z_i/Z_1$ with larger i. The alternative is calculating the normalization ratio between neighbours and using products to define y_i: $y_i = Z_i/Z_1 = Z_i/Z_{i-1} \times ... \times Z_2/Z_1$. The error in each estimator is compounded with each multiplication. We prevent this by turning the estimator equation into a matrix with weight functions α_{ij}:

$$\begin{aligned}1 &= \frac{\sum_{j\neq i}\int h_i h_j \alpha_{ij}\mathrm{d}\mathbf{x}}{\sum_{j\neq i}\int h_i h_j \alpha_{ij}\mathrm{d}\mathbf{x}} = \frac{Z_1}{Z_1}\frac{\sum_{j\neq i}\int Z_j h_i \pi_j \alpha_{ij}\mathrm{d}\mathbf{x}}{\sum_{j\neq i}\int Z_i \pi_i h_j \alpha_{ij}\mathrm{d}\mathbf{x}} \\ &= \frac{E_1(h_i\alpha_{i1}) + \sum_{j\neq i, j\neq 1}\frac{Z_j}{Z_1}E_j(h_i\alpha_{ij})}{\frac{Z_i}{Z_1}\sum_{j\neq i}E_i(h_j\alpha_{ij})}.\end{aligned}$$

We bring all dependencies on the normalization constants to one side and make the substitutions $a_i = \sum_{j \neq i} E_i(h_j \alpha_{ij})$ and $b_{ij} = E_j(h_i \alpha_{ij})$:

$$b_{i1} = E_1(h_i \alpha_{i1}) = \frac{Z_i}{Z_1} \sum_{j \neq i} E_i(h_j \alpha_{ij}) - \sum_{j \neq i, j \neq 1} \frac{Z_j}{Z_i} E_j(h_i \alpha_{ij}) \tag{7.1}$$

$$= y_i a_i - \sum_{j \neq i, j \neq 1} y_j b_{ij} \tag{7.2}$$

$$= (-b_{i2}, ..., a_i, ..., -b_{iN}) \cdot Y, \tag{7.3}$$

with E_i the expectation value in respect to probability function π_i.

We end up with the matrix equation as given by Lelièvre [1]:

$$A(\alpha) Y = B(\alpha), \tag{7.4}$$

with:

$$A(\alpha) = \begin{pmatrix} a_2 & -b_{23} & \cdots & -b_{2I} \\ -b_{32} & a_3 & \cdots & -b_{3I} \\ \vdots & \vdots & \ddots & \vdots \\ -b_{I2} & -b_{I3} & \cdots & a_I \end{pmatrix}, \; B(\alpha) = \begin{pmatrix} b_{21} \\ b_{31} \\ \vdots \\ b_{I1} \end{pmatrix}.$$

Using an estimator for the expectation values we can calculate every matrix element and invert matrix A to acquire the normalization vector Y. There is still a degree of freedom left to exploit: the weight functions α_{ij}. As Lelièvre states, we want to choose α such so the asymptotic covariance matrix is minimal. This is true for:

$$\alpha_{ij}(\mathbf{x}) = \frac{n_j y_j^{-1}}{\sum_{l=1}^{N} n_l y_l^{-1} h_l(\mathbf{x})}, \tag{7.5}$$

implying that α does not depend on i. This choice for α results in an implicit equation for Y. Instead of trying to solve for all y_i we attempt an iterative approach. We start with the assumption that every y_i is one inserting these y_i in α and solving the matrix equation 7.4. This gives us a vector Y with new values for y_i. We reuse these new values to calculate a new value of Y until convergence is reached.[2]

[2]This is not guaranteed but in practice the normalization constants convergence quickly to a stable distribution.

As an extra boon, this choice of α also allows us to circumvent matrix inversion completely. We rewrite a_i as $1 - E_i(h_i \alpha_{ii})$ by moving the sum inside the expectation value. Inserting this in equation 7.1 after moving all variables to one side yields:

$$\begin{aligned} 0 &= y_i a_i - \sum_{j \neq i} y_j b_{ij} \\ &= y_i E_i \left(\frac{\sum_{j \neq i} n_j y_j^{-1} h_j}{\sum_{l=1}^{N} n_l y_l^{-1} h_l(\mathbf{x})} \right) - \sum_{j \neq i} y_j E_j \left(\frac{n_j y_j^{-1} h_j(\mathbf{x})}{\sum_{l=1}^{N} n_l y_l^{-1} h_l(\mathbf{x})} \right) \\ &= y_i - E_i \left(\frac{n_i h_i(\mathbf{x})}{\sum_{l=1}^{N} n_l y_l^{-1} h_l(\mathbf{x})} \right) - \sum_{j \neq i} E_j \left(\frac{n_j h_j(\mathbf{x})}{\sum_{l=1}^{N} n_l y_l^{-1} h_l(\mathbf{x})} \right) \\ &= y_i - \sum_{j=1}^{N} E_j \left(\frac{n_j h_j(\mathbf{x})}{\sum_{l=1}^{N} n_l y_l^{-1} h_l(\mathbf{x})} \right). \end{aligned}$$

The dependency on n_j in the numerator disappears when replacing the expectation value with an estimator. We now have an iterative procedure to acquire y_i:

$$y_i^{k+1} = \sum_{j=1}^{N} \sum_{i=1}^{n_j} \left(\frac{h_j(\mathbf{x}_i^j)}{\sum_{l=1}^{N} n_l (y_l^k)^{-1} h_l(\mathbf{x}_i^j)} \right).$$

References

[1] Tony Lelièvre, Mathias Rousset, and Gabriel Stolz. *Free Energy Computations*. 1st. London: Imperial College Press, 2010.